University of South Bohemia in České Budějovice

Faculty of Science

Bachelor thesis

Three-Dimensional Visualization of Tick-Borne Encephalitis Virus Infection in Mouse Brain Tissue

Laboratory of Electron Microscopy

Sarah Gahbauer

Supervisor: RNDr. Marie Vancová, Ph.D.

Co-Supervisor: RNDr. Jiří Týč, Ph.D.

České Budějovice, 2023

Gahbauer, S., 2023: Three-Dimensional Visualization of Tick-Borne Encephalitis Virus Infection in Mouse Brain Tissue. Bc. Thesis, in English – p. 40, Faculty of Science, University of South Bohemia, České Budějovice, Czech Republic.

Annotation: Tick-borne Encephalitis Virus (TBEV) is an important human pathogen that causes serious neuroinfections such as inflammation of the brain (encephalitis), the lining of the brain (meningitis), and the spinal cord (myelitis). The exact mechanism by which the virus enters the brain remains an unsolved problem. However, the virus is known to infect several cells in the brain, such as glial cells and neurons. This thesis focusses on the ultrastructural changes induced by infection in the mouse brain. A special focus was placed on the endothelium during infection and to determine if or how endothelial cells can be infected to reconstruct possible entry routes of the virus into the brain.

Declaration:

I declare that I am the author of this qualification thesis and that in writing it I have used the sources and literature displayed in the list of used sources only.

České Budějovice, date .....

Sarah Gahbauer

Acknowledgements

I would like to express my greatest gratitude to my supervisor, RNDr. Marie Vancová and my co-supervisor RNDr. Jiří Týč who always supported me during the whole process of this work. They provided me with excellent guidance, patience and answers to all my many questions. I also would like to thank Martina Tesařová who took a week of her precious time to show me and my colleagues the entire sample preparation process in the lab with absolute patience and effort. Also, I would like to thank my family for the constant support and especially my mother, who helped me edit my SBF-SEM pictures. A special thanks goes out to my friends who have always been kind and supportive.

Abstract

Tick-borne encephalitis has an incidence of 10 000 to 15 000 cases of tick-borne encephalitis annually and is caused by the tick-borne encephalitis virus (TBEV), which is an important human pathogen. In addition to encephalitis, the virus can cause serious neuroinfections of the cerebral membrane and spinal cord. Since the exact mechanism of viral entry into the brain and the effect of infection on the brain still remain unsolved, this thesis is focused on the ultrastructural changes induced by TBEV infection in the mouse brain. To better understand infection in vivo, serial block face scanning electron microscopy (SBF-SEM) was used to describe and evaluate the ultrastructural changes of mouse brain cells induced by TBEV infection in 3D. I show the formation of circular structures in long processes, dendrites, and astrocyte end feet, *in vivo*. The observed whorls, which were probably created using the smooth ER as a membrane source, could be of autophagic origin and presumably support replication within proliferated parts of the ER. Furthermore, infection of astrocytes, their end feet, and pericytes is observed. These cells are very susceptible to infection, often resulting in necrosis in contrast to endothelial cells. This fact supports the hypothesis of TBEV transcytosis without endothelial cell infection. The thesis clearly shows the effect of TBEV after intracranial injection in a mouse model and provides information on the host response at the cellular level. Based on this information, further studies can be designed to examine these new findings to resolve the mechanisms associated with TBEV infection *in vivo.*

Table of Contents

List of abbreviations

BBB – Blood-brain barrier

BM – Basal membrane

BSE – Backscattered electron

BSL3 – Laboratory of Biosafety Level 3

CNS – Central nervous system

CLAHE - Contrast-limited adaptive histogram equalization: This tool works on small image regions (tiles) and enhances their contrast. In addition, it can be regulated to avoid amplification of any disturbance that might be present on the tile.

EM – Electron microscopy

GB – Gigabyte

HFW – Horizontal field width

RAM – Random-access memory

RNA – Ribonucleic acid

ROI – Region of interest

SBF SEM – Serial block face scanning electron microscopy

SEM – Scanning electron microscope

TB – Terabyte

TBEV – Tick-borne encephalitis virus

TCH – Thiocarbohydrazide

1. Introduction

1.1. Tick-borne encephalitis virus is an important human pathogen

Reaching 10 000 to 15 000 reported human cases per year worldwide (Dobler, 2010), tick-borne encephalitis represents a human viral infectious disease that affects the central nervous system and is caused by the tick-borne encephalitis virus (TBEV) (reviewed by (Kohlmaier et al., 2021)). TBEV is counted among the family *Flaviviridae* and is a member of the genus *Flavivirus* to which various crucial human pathogens transmitted by arthropods such as West Nile virus (WNV), Powassan virus (POWV), Japanese encephalitis virus (JEV), and Zika virus (ZIKV) belong (Fares et al., 2021). It is prevalent in Asia and Europe, reflecting the native habitat of its primary vectors, Ixodes persulcatus (taiga tick) and Ixodes ricinus (sheep tick) (Potokar et al., 2019) which can transmit the virus to humans in all stages of their life cycle: larva, nymph, and adult tick (reviewed by (Amicizia et al., 2013)). Regarding nonvectorial transmission of the pathogen, it has also been shown that this vector-borne disease can be transmitted when unpasteurized milk and milk products from infected cows, goats, and sheep are consumed (reviewed by (Martello et al., 2022)). Recently, the Himalayan and Baikal subtypes of the virus have also been described ((Dobler G & Tkachev S, 2021)) traditionally, TBEV has been categorized into the three subtypes Siberian, European, and Far Eastern (reviewed by (Kutschera & Wolfinger, n.d.)).

1.2. Structure of the tick-borne encephalitis virus

Holding a positive sense single-stranded RNA in its icosahedral-shaped lipid envelope, the tick-borne encephalitis virus reaches a size of 50 nm. Protected by the lipid envelope, a nucleocapsid layer surrounds the RNA that encodes a 3414 amino acid polyprotein (Sudhindra, 2018) that can be cleaved into 11 structural and nonstructural proteins in a co- and post-translational manner. The bilayer envelope that surrounds the nucleocapsid (NC) of the virus is constructed by lipids that originate from the host in which the envelope glycoprotein E and the membrane protein M are embedded, forming heterodimers (Chmielewska et al., 2022) of which 2 are assembled into heterotetramers, respectively, acting as fundamental building blocks of the virion. Besides the two structural proteins E and M, there is also a third encoded structural protein called C protein (capsid). Through the interaction of the capsid protein and the genome, the nucleocapsid (NC) is formed (Füzik et al., 2018).

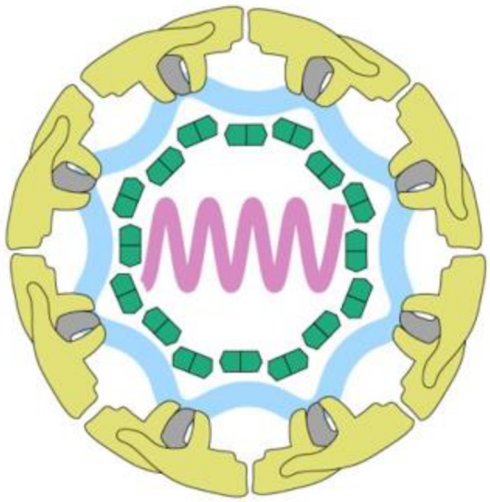

Figure 1: Structural view of the TBE virus. The single-stranded viral RNA (lilac) is encased by numerous replicas of the C protein (green) that form the nucleocapsid. On the other hand, this is framed by a lipid membrane (light blue), in which the M and E proteins (grey and yellow, respectively) are embedded (modified from (Pulkkinen et al., 2018)).

1.3. TBEV entry and replication cycle

The virus is transmitted to humans or vertebrates by the bite of an infected tick. Transmission is facilitated by tick saliva, that promotes initial replication of TBEV in skin dendritic cells (Labuda et al., 1996; Lieskovská et al., 2018) which is likely to take place in Langerhans cells (Wikel et al., 1994). These cells are found in the human epidermis and transfer viral particles through the draining lymphatics to the lymph nodes. This causes viral entry into the bloodstream (viremia) and is subsequently followed by systematic infection (reviewed by (Sudhindra, 2018)). It is also well known that for viral invasion of the central nervous system, high-level viremia is required (Mandl, 2005). For the entry of TBEV into mammalian cells, the laminin-binding protein (LBP) and the αVβ3 integrin have been considered as two main receptor candidates (reviewed by (Pulkkinen et al., 2018)).

The first step of the TBEV replication cycle (Figure 2B), which was reviewed by Mandl C. (2005), consists of the attachment of the virions to the host cell surface, which is facilitated by its E protein. Clathrin-coated pits mediate endocytosis through receptors and transfer virions to a set of intracellular membranous compartments of the host cell, called prelysosomal endocytic compartments. These vesicles possess a low pH that induces reorganization and a conformational change of the E protein from dimers to trimers, which in turn fuses the endosomal membrane with the virus. This process provokes the release of the viral nucleocapsid into the cytoplasm of the host and causes the RNA to separate from the capsid (Fusion uncoating). The now free genome of the virion is used for translation into a single polypeptide. After the polyprotein has been processed, the replication of the genome begins. The process of RNA replication involves the production of full-length negative-strand copies of the genome. These are then used to create new positive-strand RNAs. Meanwhile, translocation of the E and prM protein into the lumen of the endoplasmic reticulum (ER) is initiated followed by proteolytic cleavage of their amino-termini by host cell enzyme signalase. Subsequently, C proteins envelope RNA into nucleocapsids on the outside of the ER membrane, assembling the viral envelope through budding of the nucleocapsid into the ER. The result of this process are non-infectious 'immature' virions in which E and prM proteins form heterodimers on the viral surface (Fig. 2A).

To accomplish virus maturation, the immature viral particles are transported via the secretory pathway of the host to the late trans-Golgi network (TGN). On arrival at this site, the protease Furin cleaves the prM protein in acidic vesicles, creating the small M protein. This process enables the formation of fusion-competent homodimers as a result of reorganization of the E protein. Ultimately, the release of infectious, mature, and protein M-containing viral particles from the host cell is initiated by fusion of the plasma membrane with transport vesicles (Mandl, 2005).

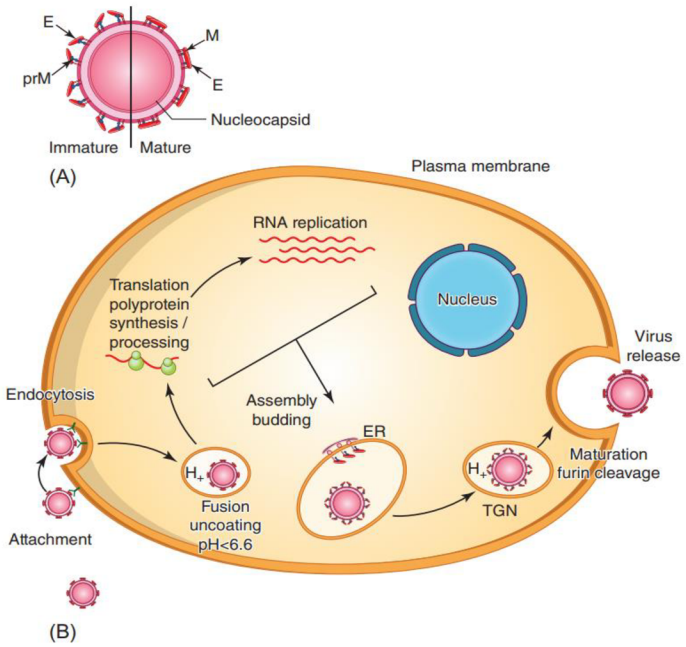

Figure 2: TBEV replication scheme. Visual representation of the immature/mature virion (A) and the viral replication cycle in the host cell (B). Reprinted from Tick-Borne Infections of the Central Nervous System, Vol 3, Kateryna Kon, Mahendra Rai, The Virus, Replication, and Pathogenesis, Page 2, Copyright (2018), with permission from Elsevier.

1.4. Virus-induced ultrastructural changes

Positive-strand RNA viruses use the cellular membranes of the host cell to promote every step of their replication during infection such as endocytosis, replication of the genome, assembly of the nucleocapsid and the release of mature viral particles. To achieve this, they cause rearrangements of (endo)membranes of their host cells to generate protective microenvironments in which replication of their genomes and the following production of new virions are supported. These environments can be called membranous replication factories (Romero-Brey & Bartenschlager, 2014) and are believed to shield the intermediates of the viral replication from the detection and the defence system of the host cell. Among others, interferon induction is thought to be delayed with the help of these environments, thereby avoiding access to cytoplasmic pathogen receptors (Överby et al., 2010). Expressing a single viral protein is often enough to induce such alterations (Nguyen-Dinh & Herker, 2021). During infection, viral proteins and hijacked proteins from the host aim to rearrange the host (endo)membrane systems. However, the detailed features of the structure and its size may differ if replication is interrupted. Furthermore, the created replication factory or the so-called replication organelle depends on the group virus that invades a cell (Fig. 3) and the source of the membrane (Nguyen-Dinh & Herker, 2021).

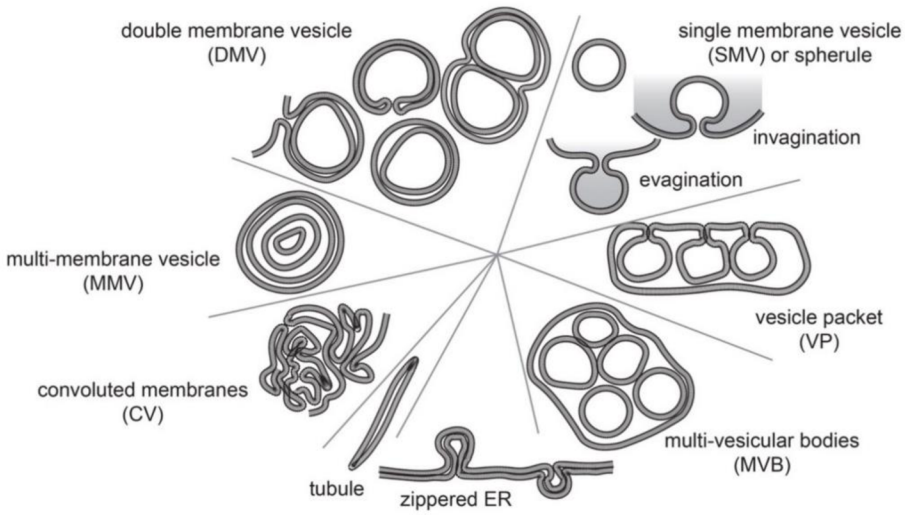

Figure 3: The most common types of membrane structures that occur in cells infected with positive-strand RNA viruses. Convoluted membranes, vesicles, and spherules in tubule-like or single membrane form are typically found during replication of TBEV (reviewed by (Nguyen-Dinh & Herker, 2021)).

For TBEV, replicated viral RNA cannot be diffused freely in the cytoplasm, but diffusion is possible within the interconnected regions of virus-induced vesicles of the altered ER compartments (Miorin et al., 2013). This rearrangement and proliferation of the rough ER in response to TBEV replication was observed in medulloblastoma and glioblastoma cells (Růžek et al., 2009). In primary human neurons, proliferated ER formed large membranous whorls and Bílý et al. suggest the formation of autophagic vacuoles containing proliferated ER with TBE virions in neural cells *in vitro*. In human neuroblastoma cells, a significant dose-dependent increase in virion production was found upon autophagy stimulation (Bílý et al., 2015). In addition to membranous alterations, the disintegration of cytoskeletal filaments has also been described (Růžek et al., 2009). Modifications in the cytoskeleton have a substantial effect on vesicle transport in the host cell, which coincides with the finding of increased mobility of vesicle transport over longer periods after infection (reviewed by (Potokar et al., 2019)) and decreased virus infectivity through dendrites/axons when microtubules were inhibited using nocodazole (Bílý et al., 2015).

1.5. Blood-brain barrier: structure, function, and role during TBE infection

The blood-brain barrier (BBB) is a term used to define the special properties of the microvasculature of the central nervous system (CNS). Vessels of the CNS can regulate molecule, cell, and ion movement between the blood and the CNS ((Zlokovic, 2008), (Daneman, 2012)). The BBB is made up of cerebral endothelial cells that are extremely thin (Coomber & Stewart, 1985) and form complex tight junctions between adjacent endothelial cells. These junctions act as a physical barrier forcing most molecules to migrate the BBB transcellularly, instead through the junctions like in most endothelia (Hawkins & Davis, 2005; Wolburg & Lippoldt, n.d.). Along the endothelium, pericytes surround the cerebral capillaries partially in a discontinuous manner (Abbott et al., 2010). They have long processes that often extend over several endothelial cells and are able to contract the capillary diameter through contractile proteins (reviewed by ((Daneman & Prat, 2015)). The pericytes and endothelium are both ensheathed by the local basement membrane that forms a perivascular extracellular matrix called basal lamina (BM) (Abbott et al., 2010). The BM is involved in many signalling processes and also forms an additional barrier for cells and molecules that aim to enter neural tissue (Daneman & Prat, 2015). The foot processes of astrocytes are connected to the capillaries and neurons, thereby establishing a complex network around them, which is crucial for the induction and maintenance of this barrier. Microglia reside in the brain and are immunocompetent cells (Abbott et al., 2010).

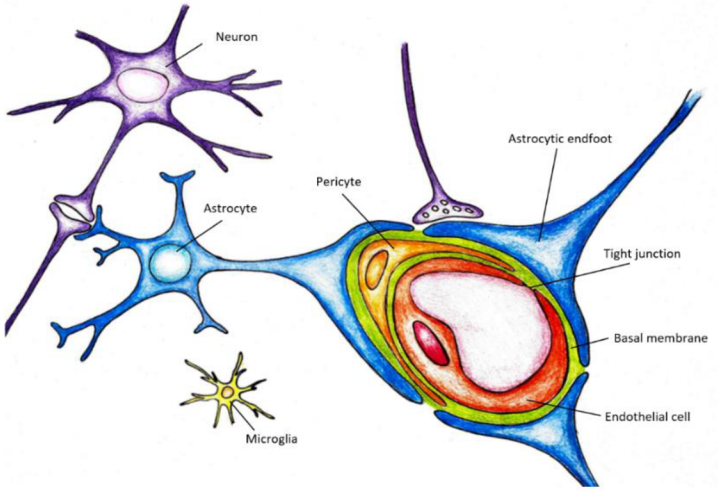

Figure 4: Schematic representation of the neurovascular unit. Its properties are largely established by endothelial cells, but are also maintained by important interactions with immune cells, mural cells such as the BM, astrocytes, and neural cells (Daneman & Prat, 2015). Figure based on description of (Abbott et al., 2010), drawing by Sarah Gahbauer.

There are three neural cell types that are especially associated with the BBB: Neurons or neurocytes are the cells which receive sensory input, send motor commands to muscle cells, and are in charge of electrical transformation in between. These cells are composed of long thin structures which generate action potentials (Axons), the cell body that contains the nucleus (Soma), and the branched dendrites, which have small spines, where neurons receive signals at their synapses from other cells. Proteins can be transported along the axons and dendrites. There are different types of neurons in the brain and also in the spinal cord (Woodruff, n.d.). Oligodendrocytes, on the other hand, form the myelinating sheath that insulates the axons in the CNS and differ in rodents and humans. As a result of their unique physiology and their complex differentiation pathway, these cells are very vulnerable. Myelination and maintenance of myelin sheaths are very complex and therefore can be disturbed by diseases of the nervous system (Bradl & Lassmann, 2010). Astrocytes are tightly associated with the BBB and are abundant heterogeneous neuroglial cells in the CNS. They are thought to be the main providers of homeostasis in the brain and support neuronal functions by controlling the levels of neurotransmitters, ions, and regulating synaptogenesis. They also maintain the blood barrier and remove waste material since they occupy a large part of the brain parenchyma where they enwrap synapses (reviewed by (Potokar et al., 2019)).

The BBB has many crucial functions in the brain. One of them is the maintenance of ionic homeostasis and brain nutrition. Ion concentration and pH are tightly controlled by a combination of specific transporters and ion channels, which ensure synaptic and neural signalling functions (reviewed by ((Kadry et al., 2020)). Furthermore, the BBB is responsible for the regulation of neurotransmitters. The CNS and peripheral nervous system often use the same neurotransmitters. The BBB keeps those transmitter pools separate, which minimizes 'crosstalk' and keeps plasma levels constant (Abbott et al., 2006; Bernacki et al., 2008). The BBB also offers protection against neurotoxins and limits the leakage of plasma macromolecules into the brain, resulting in control of protein content in cerebrospinal fluid (Abbott et al., 2010). This is important because leakage of plasma proteins such as albumin through a damaged BBB can induce nervous tissue apoptosis due to cell activation ((Nadal et al., 1995), (Gingrich & Traynelis, 2000)).

It is not yet fully understood how the breakdown of the blood-brain barrier is associated with TBEV infection, nor the exact process of virus entry into the CNS. There are several hypotheses on how TBEV attains the brain in humans: One possibility is the direct entry of the virus through the olfactory nerve or the virus could use the breakdown of the BBB to invade in a hematogenous manner. It is also possible that the virus enters through infected BBB cells (McMinn, 1997), (Koyuncu et al., 2013). The West Nile virus (WNV) and TBEV have the ability to cross the blood-brain barrier using transcytosis and through infected leukocytes, which is called the 'Trojan horse' route. Some flaviviruses such as Zika virus (ZIKV), Japanese encephalitis virus (JEV), WNV, and TBEV might cross as a cell-free virus after systematic infection, leaving the neurovascular unit with no noteworthy cytopathic effect (reviewed by (Bhide et al., 2022)). However, Růžek and colleagues found that the permeability of the blood-brain barrier was increased in later stages of virus infection when a high virus load resided in the brain but the disruption of the BBB was not a mandatory step for CNS invasion (Růžek et al., 2011). Furthermore, Stamatovic et al. proposed that the BBB can be disrupted by other mechanisms than endothelial cell infection(Stamatovic et al., 2005) They found that virally induced production of certain chemokines, such as monocyte chemoattractant protein 1 (MCP-1, CCL2) caused the alteration of tight junction proteins and, therefore, their permeability . MCP-1 is one of the most expressed chemokines during CNS inflammation (Mennicken et al., 1999).

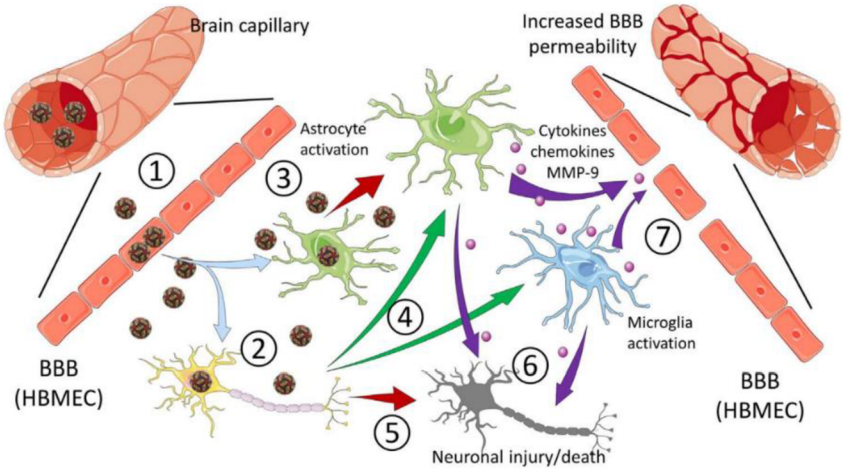

Figure 5: Possible entry of TBEV, induction of neuroinflammation, and breakdown of the BBB. Throughout viremia, the virus might infect primary human microvascular endothelial cells (HBMECs) and release new virions into neural tissue without compromising BBB integrity (1). In addition, other mechanisms could be involved. The primary target of infection represents the neurons in the CNS (2). Astrocytes may be activated due to supporting the replication of TBEV (3). Neurons that have been infected produce cytokines that activate microglia and astrocytes (4). Neuronal injury or death is caused by TBEV infection (5). Microglia and activated astrocytes produce large amounts of chemokines, cytokines, and MMP-9 that are thought to have neurotoxic effects (6) and can induce the breakdown of BBB (Palus et al., 2017). This figure was used with permission from the authors (Palus et al., 2017).

1.6. Pathogenesis of TBEV infection

As a zoonotic virus, TBEV infections are often minimally pathogenic in their natural hosts, but can be neuroinvasive and highly virulent in hosts that are not natural. The lethality and virulence of zoonotic infections may be caused by the cytokine storm induced in response to the primary infection (Teijaro et al., 2011). In humans, it therefore can cause serious neuroinfections such as inflammation of the brain (encephalitis), the lining of the brain (meningitis), and the spinal cord (myelitis) (Potokar et al., 2019).

Infections with different subtypes of TBEV have shown a different clinical appearance ((Dobler et al., 2021); (Bogovic, 2015)). It was found that CNS inflammation is followed by a febrile disease in most patients who were infected with the European subtype of TBEV and resulted in a biphasic course of the disease. The first phase of the disease usually takes less than one week and is associated with viremia. It is characterized by fever, headache, and muscle/joint pain. These symptoms arise in the absence of CNS inflammation (reviewed by (Bogovič, Kastrin, Lotrič-Furlan, Ogrinc, Županc, et al., 2022). The first phase is then preceded by an improvement which lasts several days. The second phase then begins, which involves the CNS, whereby mostly meningitis predominantly affects children and approximately half of adult patients. Meningoencephalitis and meningoencephalomyelitis also occur (Bogovič et al., 2022; Bogovic et al., 2015). Compared to other virally induced CNS inflammation, TBE is more severe on average, and its fatality rate is up to 1% in patients infected by the European subtype. In addition, 5% of the patients suffer permanent paresis and 30% experience postencephalitic syndrome (reviewed by (Bogovič, Kastrin, Lotrič-Furlan, Ogrinc, Avšič Županc, et al., 2022)). In fact, there are unique problems in the treatment of patients affected due to the complex feature of the CNS, which has limited regeneration capacity and reduced immune surveillance. TBE infection, as well as other neurotropic viruses, irreversibly damage the CNS in its functional and structural architecture, also through the virally induced local immune response (Ludlow et al., 2016). To gain a better understanding of the ultrastructural changes induced by viral replication and to determine the role of the BBB during infection, we used a mouse model to investigate TBEV infection *in vivo*.

1.7. Serial blockface imaging

The term Serial blockface imaging, to which Serial Blockface Scanning Electron Microscopy (SBF SEM) is counted, refers to electron microscopy techniques recording image data immediately from the surface of a specimen that is situated in the chamber of a scanning electron microscope (Deerinck et al., 2010), (Tapia et al., 2012). Tissue which was previously impregnated with heavy metals and then embedded in epoxy resin is mounted within a scanning electron microscope (SEM). The microscope contains an ultramicrotome, which a device that can cut very thin slices, that holds a built-in diamond knife. After it cuts a flat surface from the specimen block and retracts again, the block is scanned in a raster pattern with an electron beam. This results in a picture of the tissue ultrastructure. The block is raised by a specific z-value and a new surface can be cut. Repeating this process, a three-dimensional (3D) block of images is constructed (Courson et al., 2021).

The generation of the signals for the images is dependent on backscattered electrons that are produced when elements of high atomic number such as lead, osmium, and uranium are hit by an electron beam (Deerinck et al., 2010). Therefore, heavy metal impregnation ensures the conductivity and maximal contrast of the tissue (Tapia et al., 2012). In addition to metal impregnation, the use of conductive epoxy resin also enhances the conductivity of the specimen (Deerinck et al., 2010). In SBF SEM, a lateral resolution of approximately 5 nm^2 and a minimum slice thickness of about 25 nm can be achieved for most biological systems. Covering a range from 1000 nm^3 to over 1 000 000 nm^3, the total volume that can be examined can be used to study various specimen types such as whole cells or collagen fibres. Even larger volumes can be achieved by the so-called stitching of multiple overlapping images to expand the visible area (reviewed by (Peddie & Collinson, 2014)).

2. Work aims

- Literature review
- Sample Preparation
- Data Acquisition using Serial block face scanning electron microscopy (SBF-SEM)
- Data processing and analysis using Microscopy Image Browser (stitching, alignment, contrast)
- Data interpretation - Based on the acquired data; to describe and evaluate the ultrastructural changes of mouse brain cells in response to TBEV infection in 3D

3. Materials and Methods

3.1. Tissue Preparation for Electron Microscopy

Infectious virions (10 plaque forming units) of a highly virulent strain (Hypr) of tick-borne encephalitis virus (TBEV) were injected intracerebrally into 1 week old ICR mice. The brain of infected mice was examined 4 days after infection (DPI). Infection of mice, including the removal of their infected brains, was carried out by Martin Palus at the BSL3 Laboratory of Arboviriology, Institute of Parasitology, ASCR Centre for Biology.

3.1.1. Chemical fixation

To prepare a sample for SBF-SEM, the brain tissue was fixed in 2.5% glutaraldehyde (SPI) and 2% formaldehyde (Polysciences) in 150 mM sodium cacodylate (Sigma C5670) (pH 7.4) together with 2 mM calcium chloride. Subsequently, the tissue obtained by dissection was cut into pieces roughly smaller than 0.5 mm^3 in size using two scalpels in a manner similar to how scissors work to minimize compression during cutting. To prepare the solution, 2g of paraformaldehyde is dissolved in 40 ml of water heated to 65 ° C and approximately 10-20ul of 10N sodium hydroxide are added to clear the solution. Subsequently, the solution was cooled to room temperature and 50 ml of 0.3M sodium cacodylate with 4 mM calcium chloride (pH 7.4). Lastly, 10 ml of 25% glutaraldehyde is added and the pH is tested. 50 ml of fixative solution per mouse brain infected with TBEV was used. To incubate and fix the tissue, the sample was first left at room temperature for 6 h and then stored in the fixative solution at 4 ° C until further preparation of the EM sample.

3.1.2. Washing, Post-fixation, and Staining

The first step consisted washing the sample with 150 mM cacodylate buffer exactly five times: The pieces obtained are placed in glass bottles together with 10 ml of the prepared buffer and shaken on a shaker. In between each rinsing process, the solution around the sample tissue is exchanged with 10 ml of fresh 150 mM cacodylate buffer by pouring and aspiration is also possible. To employ the osmium tetroxide-thiocarbohydrazide method developed in 1960 by Hanker and Seligman, the cacodylate buffer around the sample was subsequently exchanged with 4% osmium tetroxide (https://www.2spi.com/), and 3% potassium hexacyanoferrocyanide (II) trihydrate puriss (Sigma-Aldrich, 31254).

Next, a Thiocarbohydrazide (TCH) solution was prepared: An equal amount of 3% hexacyanoferrocyanide (II) trihydrate was combined in 0.3M sodium cacodylate buffer with 4 mM calcium chloride and 4% osmium tetroxide in water. The sample was incubated for 2h at room temperature. To dispose of the cacodylate buffer, a special waste bottle is used (Polaron Equipment, 2402/6). To prepare 10 ml of a 3% potassium hexacyanoferrate (II) trihydrate solution, 0.3 g must be weighed in a 125 ml beaker and mixed with 10 ml of 0.3M cacodylate buffer. The solution was stirred in a magnetic stirrer with aluminium foil on the top of the beaker until all solid parts had dissolved. When 2 h had passed, the sample was washed 3 times with cacodylate buffer, allowing the sample to incubate 3 min at room temperature between each washing step. Next, a 1% TCH solution was prepared by mixing 0.1g of TCH (Sigma) with 10 ml of water and mixing it every 10 min after the solution was slightly heated for 1 h. As soon as everything was dissolved, the solution was filtered using a 2um filter disc and the sample was immersed in it for 1 h. After incubation in the TCH solution, the sample was washed again 5 times with double distilled water for 3 min each. For the next post-fixation step, a 2% osmium tetroxide solution is required. To reach this target concentration, the initial 4% solution was mixed in a 1:1 ratio with double distilled water before incubation of the sample in this solution for 30 min at room temperature. Following this process, the samples were again rinsed 5 times in double distilled water and incubated for 3 min each between exchanging the solution at room temperature. The osmium waste was also stored in special waste bottles. Next, a 1% uranyl acetate solution was prepared by dissolving 0,1g of uranyl acetate (EMS, 22400) with 10 ml of water, mixing for about 2 hours and filtering 3 times over filter paper. After the washing step with water, the sample is placed in a 1% uranyl acetate solution and stored in the refrigerator at 4°C overnight. The next day, the sample was washed again five times with double distilled water, incubating the sample for 3 min between each washing step. Subsequently, Walton's lead aspartate solution is prepared, consisting of two chemicals and water. 0.998 g of L-aspartic acid (Serva, 14180) were dissolved in 250 ml of double distilled water and the pH of the resulting solution was adjusted to approximately 3.8 using hydrochloric acid, 1N potassium hydroxide, and pH test stripes. To this solution, 0.066 grams of lead nitrate (Analar R 672073) were added and stirring was applied until a homogeneous solution was obtained. The pH was checked again with the stripes and adjusted to a value of approximately 5.5. This solution was then used to incubate the sample in it for 30 min in the laboratory oven at 60°C. After this step, the sample was left for 2 h to let it cool to room temperature. Washing followed, where each of the five washing steps compromised a 3 min incubation time using double distilled water.

3.1.3. Dehydration

Following the staining process, dehydration was achieved using an ascending series of acetone concentrations (30-50-70-80-90-95-100-100%). The sample was immersed in 10 ml of 30% acetone solution, second in 10 ml of 50% acetone solution, and last in 10 ml of 70% acetone solution. At this point, the dehydration process can be interrupted, whereby the samples are stored at 4 °C overnight. In between exchanging the solution, the sample was left on the shaker for 15 minutes each at room temperature. To continue the process, this procedure was repeated using 10 ml of 80% acetone, subsequently 90%, then 95% and finally 2 times 10 ml of 100% acetone solution. In between each solution-exchanging step, the sample was left on the shaker for 15 minutes each at room temperature.

3.1.4. Resin Infiltration and Embedding

The dehydration procedure was then followed by infiltration with Hard Plus Resin 812 (EMS, 14115). This was completed in 4 steps: First, the sample is placed in a 25% mixture of resin from the Hard Plus Resin 812 kit (Table 1) and 100% acetone. Since this is a pre-mixed kit, all components are pre-measured and only need to be combined according to the manufacturer. Each kit includes five mini-kits, each yielding about 100g of resin. The resin is prepared according to the manufacturer and stored in the freezer using plastic syringes until further use. Before use, the resin-defrosted syringe can only be opened when room temperature is reached. To infiltrate, the sample is submerged in the 1:3 resin-acetone mixture for 2 h. Subsequently, this step was repeated 2 times. Firstly, a 1:1 mixture was implemented and, second, a 75% mixture of resin and 100% acetone solution was used. The incubation time for the 50% mixture was 2 h, and for the 75% mixture it was 3 h at room temperature. Subsequently, the sample was stored in pure resin overnight on a shaker. Finally, the infiltration process was completed by replacing the resin once more with 100% fresh Hard Plus Resin 812 and incubating for 6 h at room temperature.

Table 1: Hard Plus Resin Kit Contents

5 x 50g	Hard Plus Resin-812
5 x 50g	Hardener Hard-Plus
5 x 2.5ml	Accelerator
1x	Hard-Plus Resin-812 Kit

3.1.5. Embedding and Curing

The next day, a flat mold was filled with pure resin. The sample was carefully removed from the bottle and transferred to the mold. To label each, a small piece of numbered paper was also pushed into the molds next to the sample. Resin polymerization was performed, by placing the mold in the oven at 62 ° C for 48 hours.

3.2. Trimming and Mounting of the samples

Once the resin had been polymerized, the small block, containing the sample was trimmed with a glass knife to a size of 400 µm × 400 µm × 400 µm using the Ultramicrotome Leica EM UC6. The microtome sectioning speed was set at 100mm/s and the section thickness was adjusted to 500 µm. The block was detached from the rest of the block using a razor blade. Hereby, it is important that the tissue must be exposed on all six sides. The acquired block was attached to 7 mm aluminium specimen stubs (Agar Scientific) using a cyanoacrylate glue. As soon as the sample block was in place, the connection between the stubs and the block was coated with conductive silver liquid (EMS) and allowed to dry overnight. Subsequently, the sample on the pin was further trimmed to a size of 200 µm × 200 µm × 200 µm using a glass knife. To improve the conductivity of the sample, the entire sample on the pin was sputter coated with gold (Leica EM ACE200 vacuum coater) for 3 min under rotation to ensure a uniform coating. Before the actual imaging process, a glass knife was used to cut off the first 10-20 µm from the top of the block. The trimming and mounting procedure for the samples was conducted by a technician of the Laboratory of Electron Microscope.

3.3. Data Acquisition

Jiří Týč Ph.D. and Tamara Leutgeb (JKU) performed the imaging process using the SBF-SEM Apreo microscope (Thermo Fisher Scientific) using the BSE mode at 3 kV. The other parameters are visible in Table 2. In total, 1.5 TB of data was collected.

Table 2: Microscope Settings

Region of interest	**ROI1, ROI2, ROI3**	**ROI4 & 5**
Detector	T1	T1
Mode	volume scope	volume scope
Number of energies	2	1
Voltage	2.04 kV, 3.09 kV	2.7 kV
Depth approx.	25 nm, 50 nm	40nm
WD	6.4011 mm	6.4011 mm
Current	50 pA	50 pA
Pressure	High vac.	High vac.
Tiles	1x1	1x6 & 1x5
Pixel size	6 nm	4 nm
Dwell time	1 us	1 us
Electron dose	17.3 e/nm^2	19.5 e/nm^2
Slice thickness	50 nm	50 nm
HFW	36.864 µm	36.864 µm
Resolution	6144x4096	6144x4096
Magnification	3445x	3445x
Cut speed	0.2 mm/s	0.2 mm/s
Contrast	71.87	71.87
Brightness	32.27	32.27
Denoising: Median Filter	1	1
Normalization Clipping	5	5
Tile Track Registration	affine	affine

3.4. Data sets

In total, five datasets were examined that were distributed over the sample block in as shown in Fig. 6:

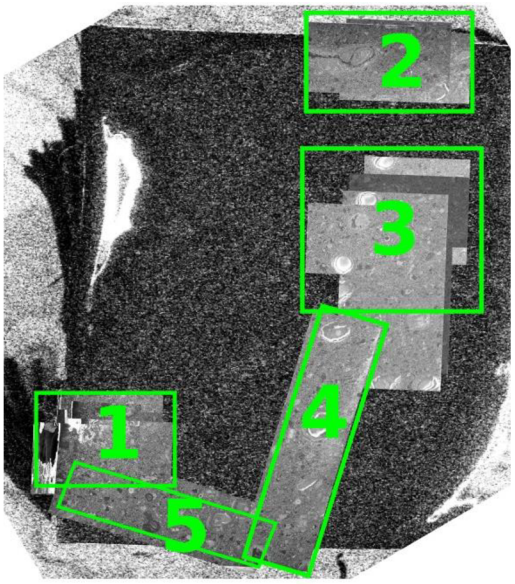

Figure 6: Distribution of data sets 1 to 5. Green squares mark each of the five regions of interest examined. Data sets 4 and 5 are substantially larger than the other ones. The region of interest 2 is the only one that does not overlap with any of the other regions.

Table 3: Dimensions of the Regions of Interest and Image Processing

	ROI 1	ROI 2	ROI 3	ROI 4	ROI 5
Slices A,B,C,D,E,F, G	A15, B992, E9, F453, G15, H714	A12, B993, E9, F453, G726	A8, B514, C2, D184, E18, F906, G484	242	242
Total Slices imaged	2198	2193	2114	242	242
Slice thickness	25nm optical, 50nm physical	25nm optical, 50nm physical	25nm optical, 50nm physical	50 nm	50 nm
Tiles	1x1	1x1	1x1	6x1	5x1
De-convolution	yes	yes	yes	no	no
Image Processing	yes	yes	yes	no	no
Segmentation/ 3D model	no	no	no	yes	yes
Images after alignment	1500	1495	1496	241	241
Damaged Areas Found	111	244	307	101	101

3.5. Data processing and analysis using Microscopy Image Browser

Analysis was carried out using the open access software Microscopy Image Browser (MIB), which was developed by I. Belevich et al. at the University of Helsinki (http://mib.helsinki.fi). The software enables visualization, editing, and segmenting of light- and electron-microscopy image datasets at a high-performance level (Belevich et al., 2016). It was especially useful for this experiment, since multidimensional image processing (3D) was possible, as well as the creation of a 3D model. When working with larger datasets (in this case several Terabytes), such as ROI1 to ROI5, a powerful PC is necessary to be able to work with the programme running smoothly. For this reason, the Laboratory of Electron Microscopy is in possession of a 128 GB RAM PC that I used for the entire data evaluation process.

3.5.1. Data Editing and Stitching

To create a 3D model of the two subregions Tile 5 and 6 of ROI4, I inverted the whole stack (3D) in the MIB and applied the Contrast-limited adaptive histogram equalization (CLAHE) tool and applied the following settings: stack (3D), number of tiles 8 8, clip limit 0.01, NBins 512, distribution Rayleigh, alpha 0.4 as well as the median filter to reduce any noise. We decided to stich ROI4 and ROI5 together, since they overlap, and the analysis process would be simplified. I opened tiles 5 and 6 from ROI4 in MIB, applied the median filter, and rotated it 90 degrees with the rotation tool. For the fifth tile of ROI5, I repeated this process, after I inverted the image stack and applied the CLAHE tool. Subsequently, I stitched these two datasets together using the application ImageJ. To create a single dataset, I imported the prepared data sets via the file tool, selected 'import,' 'image sequence,' and finally 'virtual stack.' Then I proceeded with the tool 'File' again, chose 'new', and then 'trackEM2 (blank)'. In the window that opened after this command, I clicked the right mouse key and imported both stacks. As soon as both stacks had loaded, I clicked on the right mouse key again, chose 'align', and then 'multilayer mosaic' where I kept the default settings. Ultimately, I defined the first and last slices before starting the stitching process. When finished, the data set could be exported as a flat image and saved.

4. Results and Discussion

In total, I analysed five datasets that compromised 4731 images and took pictures of 763 damaged areas. Since it would go beyond the scope of this thesis to describe and analyse all 763 images, capillary areas were preferred. In total, the volume studied compromised approximately 203 435.5 μm^3. The aim of this project was to determine how the damage caused by TBEV presents itself in the mouse brain. A special focus was placed on the endothelium to determine whether and how endothelial cells can be infected to reconstruct possible entry routes of the virus into the brain.

4.1. TBEV- induced brain tissue alterations and their presumable formation – a rodent's view

Although understanding the pathogenicity of TBEV is of great importance for the development of possible therapies for the disease, detailed information about the mechanisms of entry and replication of this virus in the brain in vivo is still unknown. Therefore, a mouse model was used to examine and describe the ultrastructural changes in the brain in response to TBEV replication.

In long processes (dendrites and axons), I observed viral replication only within the proliferated parts of the rough ER (Fig. 7), and the centres of ER whorls (multiple concentric layers of membranes) (Figs. 9-11). In the long projections, either single or multiple whorls were observed at different stages of their presumable formation (Fig. 7, 9A, 9B, 9C). I found elongated ER cisternae containing virions, which I assumed as the presumable initial stage of the whorl formation (Fig. 7; arrowhead). The proliferated empty ER cisternae were stacked together (Fig. 9A-C, 10A-C) and probably further reorganised to form multilayered concentric structures (Fig. 9D-F) that completed separation of the inner space by ER membranes. In some whorls, the peripherally located membranes were very tightly stacked (apposed) (Fig. 9E, 9F) and ranged from approximately 1 µm to 5 µm in outer diameter. Whorls spatially segregated viruses within the ER cisternae in cell bodies, as well as in the processes of neural and glial cells (Fig. 8, 9A). The centre of several observed whorls contained not only sequestered ER cisternae with virions, but also other organelles and was sometimes accompanied by necrosis or degradation of its internal contents (Fig. 11, 12, 15). In several cases, membranes forming ER whorls showed very high electron density, lost the circular profile, suggesting that these structures probably fused with lysosomes (Fig. 12C). Other whorls were electron dense throughout most of their internal structure and probably contained digested structures (secondary lysosomes) or

contained material that could not be further degraded (residual bodies) (Fig. 12A, B). These whorls were often accompanied by disintegration of other parts of the cells, often damaged the plasma membrane followed by the release of the cytoplasmic content (electron-lucent "empty" areas marked by arrowheads in Fig. 12F). The whorls were surrounded by empty areas, suggesting necrosis of a whole projection or cell body (Figs 9B, 11, 12, 15). In some projections, the remaining part of the cytoplasm of the affected dendrites and cells appeared mostly empty, but sometimes alterations in mitochondria (Fig. 12E, 14D, 20E) occurred (arrowheads), whereby it is unclear whether the observed mitochondrial holes in Fig. 12E are related to infection. I observed ER sequestration and the presence of double membranes (or more) membranes encircling the whole volume of this whorled structure, which identified them as phagophores that enclosed autophagosomes and fused with lysosomes at different advanced stages of this process (Fig. 12A-F). ER whorl engulfment and fusion with lysosomes can be identified (Fig. 12 C) whereby also necrosis is also shown here (Figs. 12A-F).

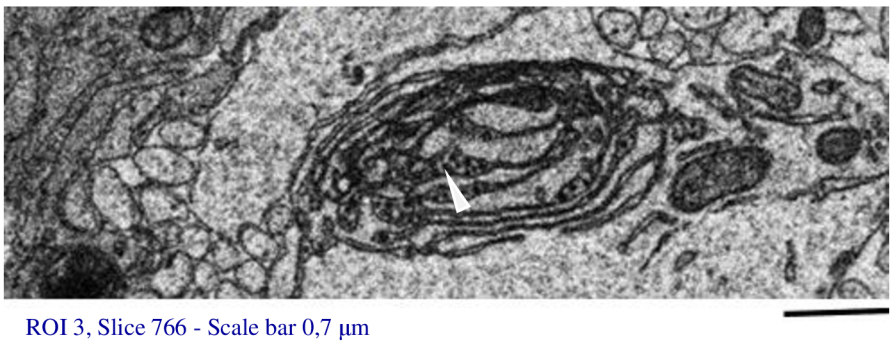

Figure 7: *In vivo* TBEV infection of brain tissue (Hypr strain, 4 DPI). Virions are visible inside the proliferated ER cisternae (arrowhead).

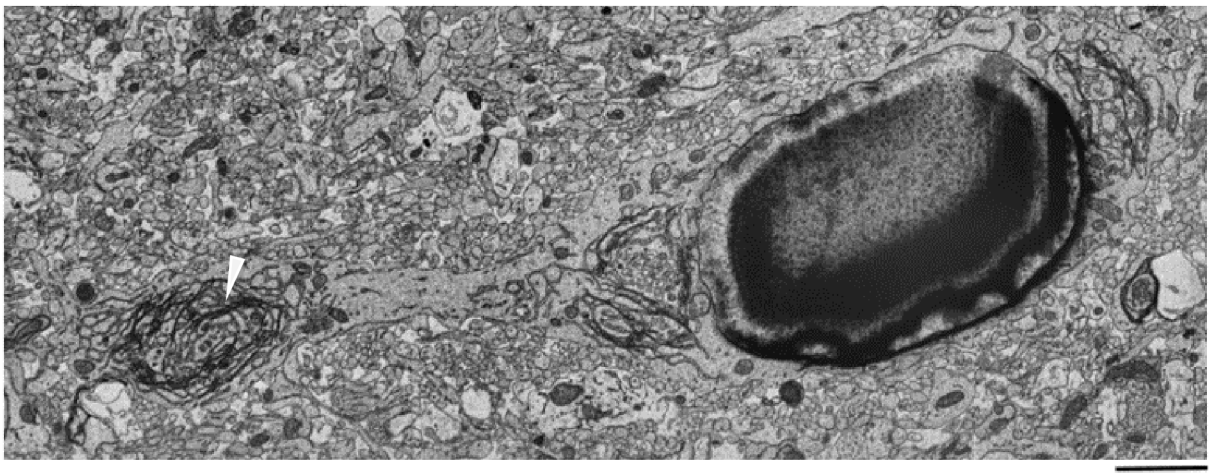

ROI 3, Slice 1246 - Scale bar 2,15 µm

Figure 8: ER Alterations that form in response to TBEV infection in the body of an infected astrocyte. ER stress can be clearly observed in the cell soma, as well as in its process (arrowhead).

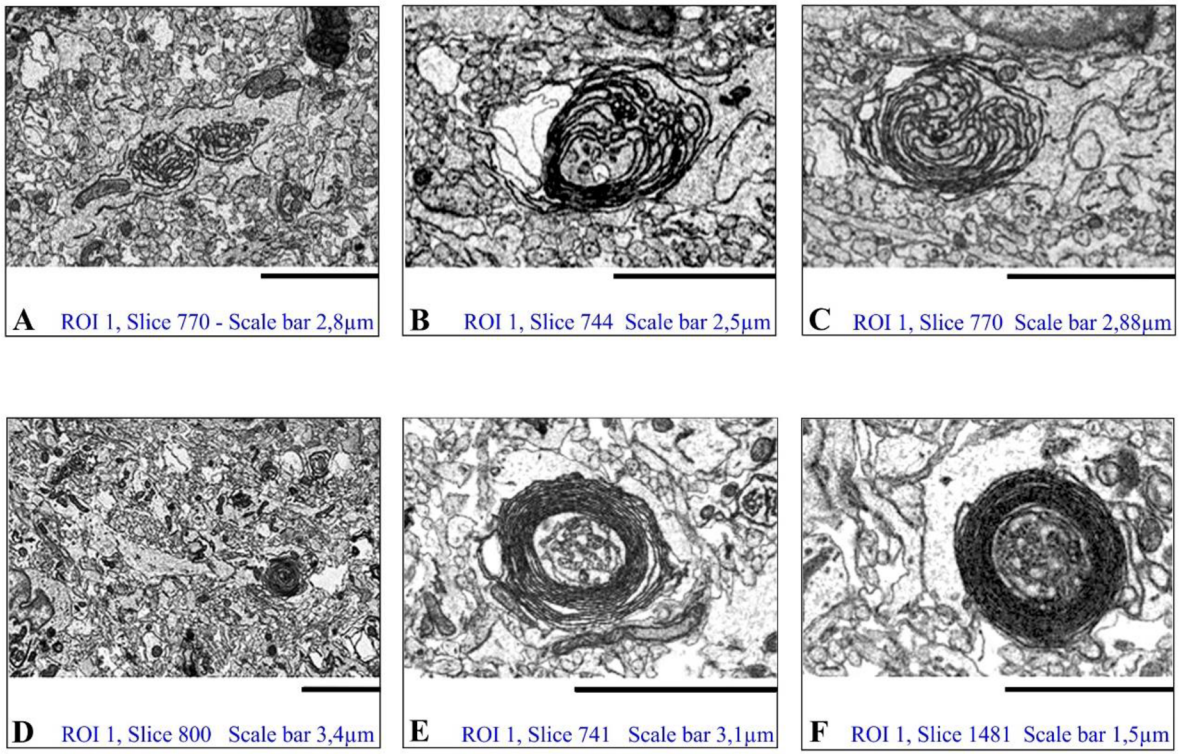

Figure 9: Presumed stages of formation of convoluted structures (whorls) inside long protrusions (ROI1). A-C shows the proliferated ER, in D-F tightly apposed highly dense membranes surrounded by altered cytoplasm at low (D) and high magnification (E,F). Whorls reside in long processes that are not in proximity to the capillary.

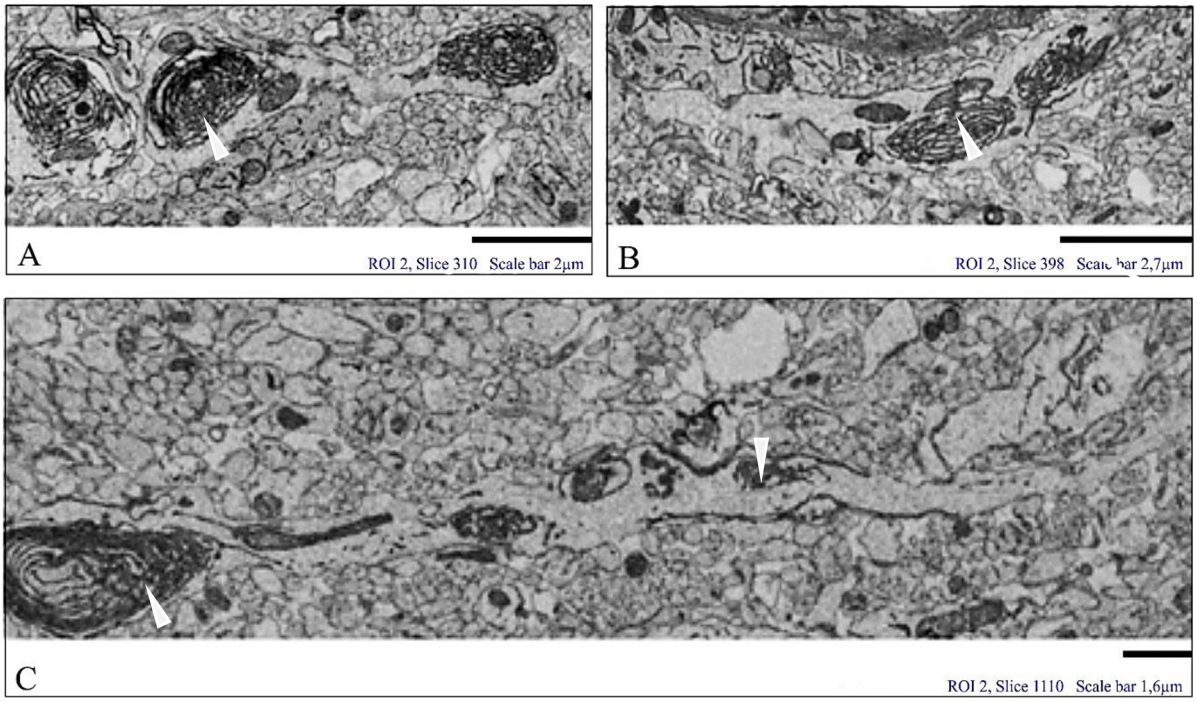

Figure 10: Multiple convoluted structures (whorls) were present inside long protrusions, probably dendrites, that run close to the capillary (ROI2). Whorls are marked by arrowheads

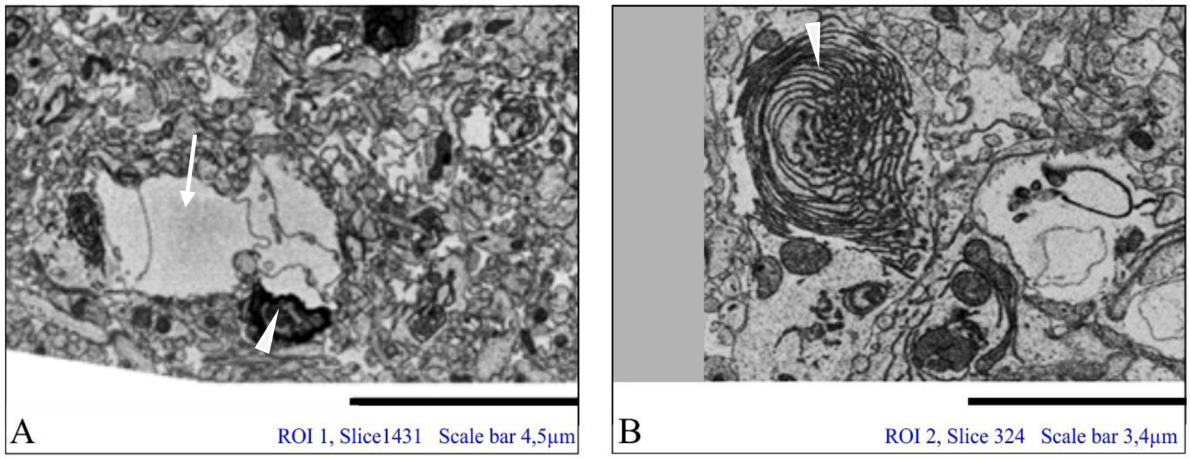

Figure 11: The proliferation of the ER is sometimes accompanied by necrosis (ROI1, ROI2). Very often, circular structures (arrowheads) could be observed with very large necrotic parts (arrows) next to them connected with a loss of plasma membrane integrity.

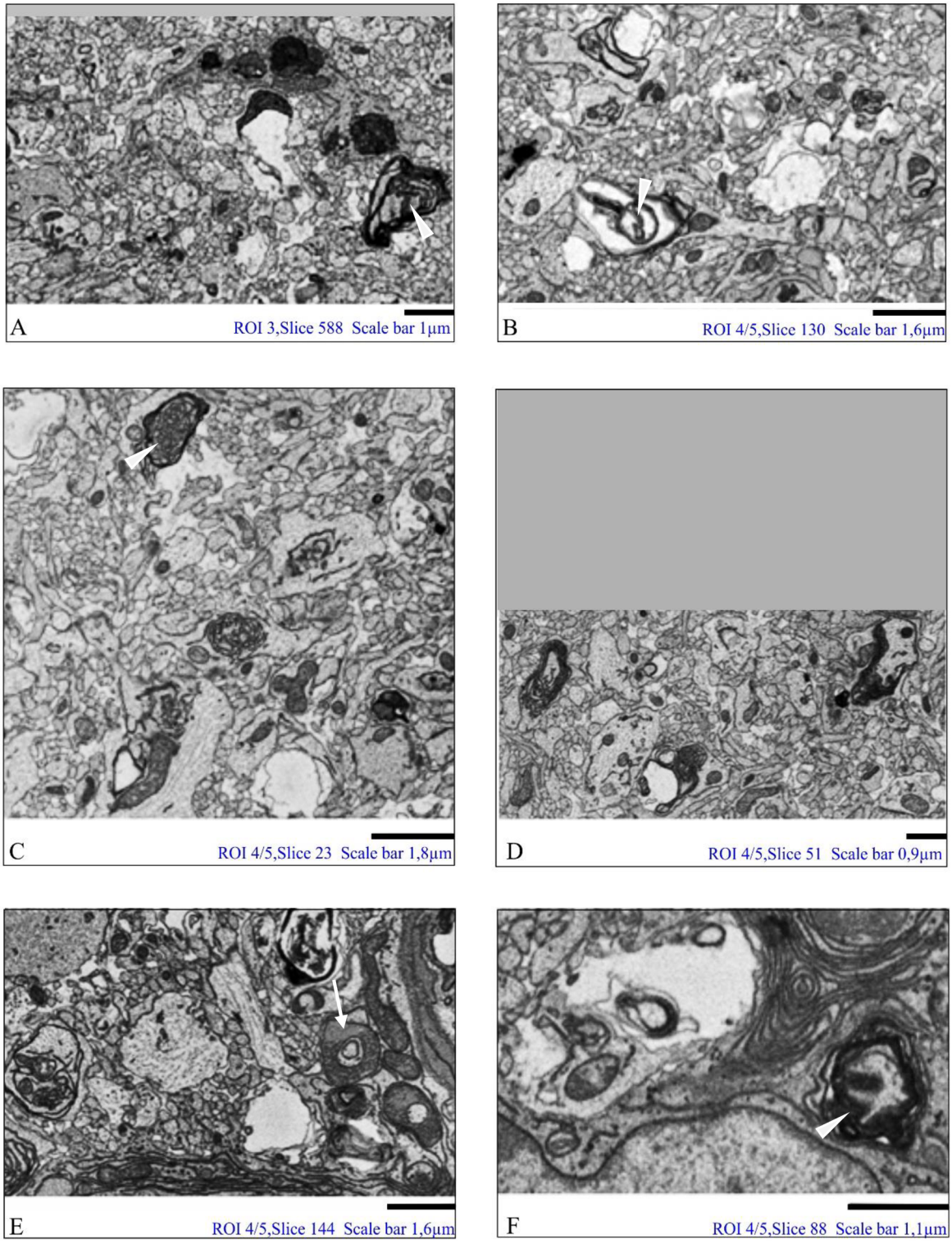

Figure 12: *In vivo brain* TBEV infection (ROI3 A), (ROI4/5 B, C, D, E, F). ER material transited to lysosomes (arrowheads). In Fig. 11E, the engulfed ER compartment resides next to the capillary and mitochondria, which appear in a shape with a cavity inside them (arrow). Figure 11F shows the proliferation of the ER accompanied by necrosis. On the right, an ER whorl is visible after lysosomal fusion (Fig. 12F, arrowhead).

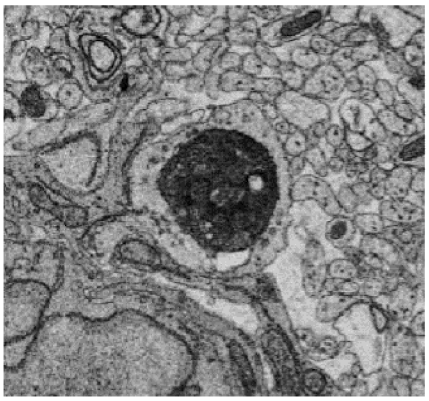

Figure 13: ER to lysosome-associated degradation. Presumed last stage after lysosomal fusion is visible, where the inner contents of the lysosome are digested.

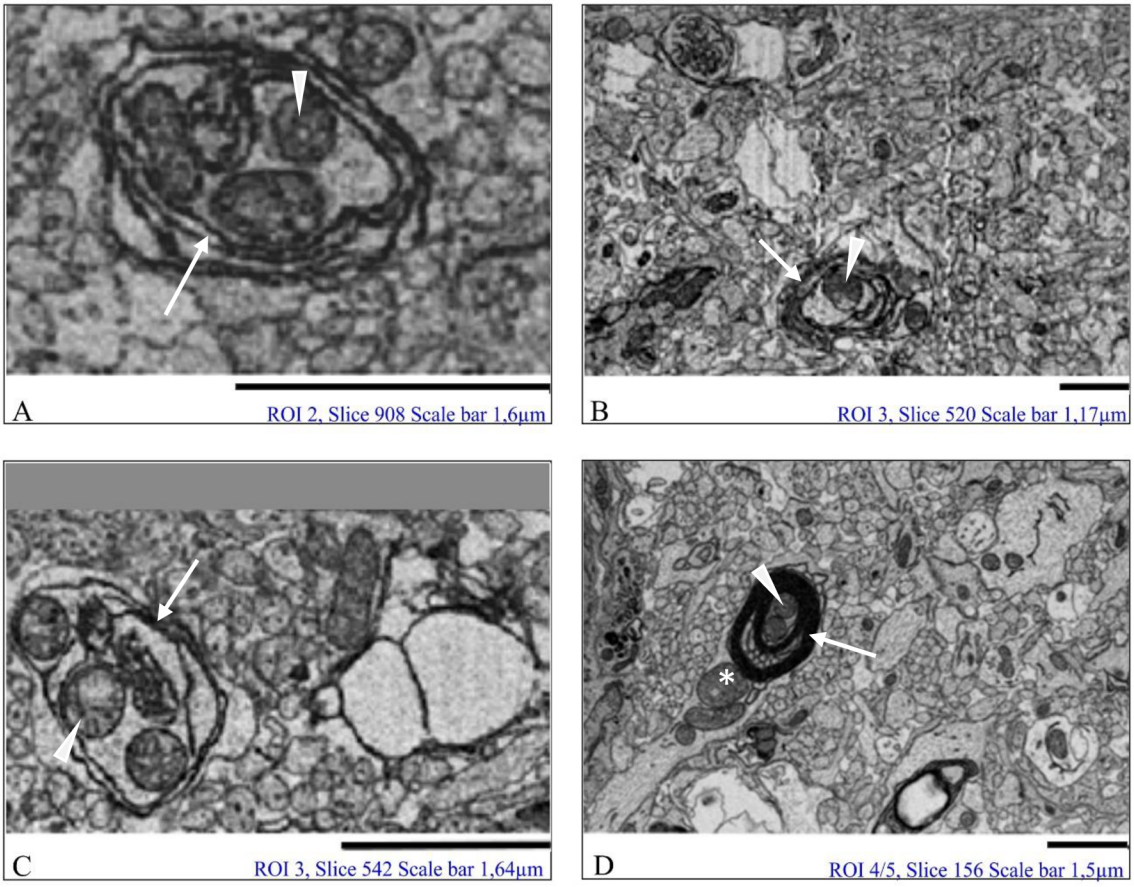

Figure 14: Autophagosomes (ROI2 A), (ROI3 B, C) (arrows) containing mitochondria (arrowheads) (ROI4/5 D). Figure 14D shows a membranous whorl residing in a dendrite that contains two swollen mitochondria (asterisk).

Microscopic signs of necrosis, such as swelling of the mitochondria or loss of membrane integrity, were abundant throughout the entire sample volume. In Fig. 15, necrotic cells are shown in brain tissue that is not in direct proximity to the capillary from the initial stage of necrosis (Fig. 15A) over necrosis accompanied by secondary lysosomes (arrowheads) in a cell that is probably an astrocyte that later connects to the capillary (Fig. 15B, 15C) until to the point where only a part of the cell survived (Fig. 15D, arrowhead).

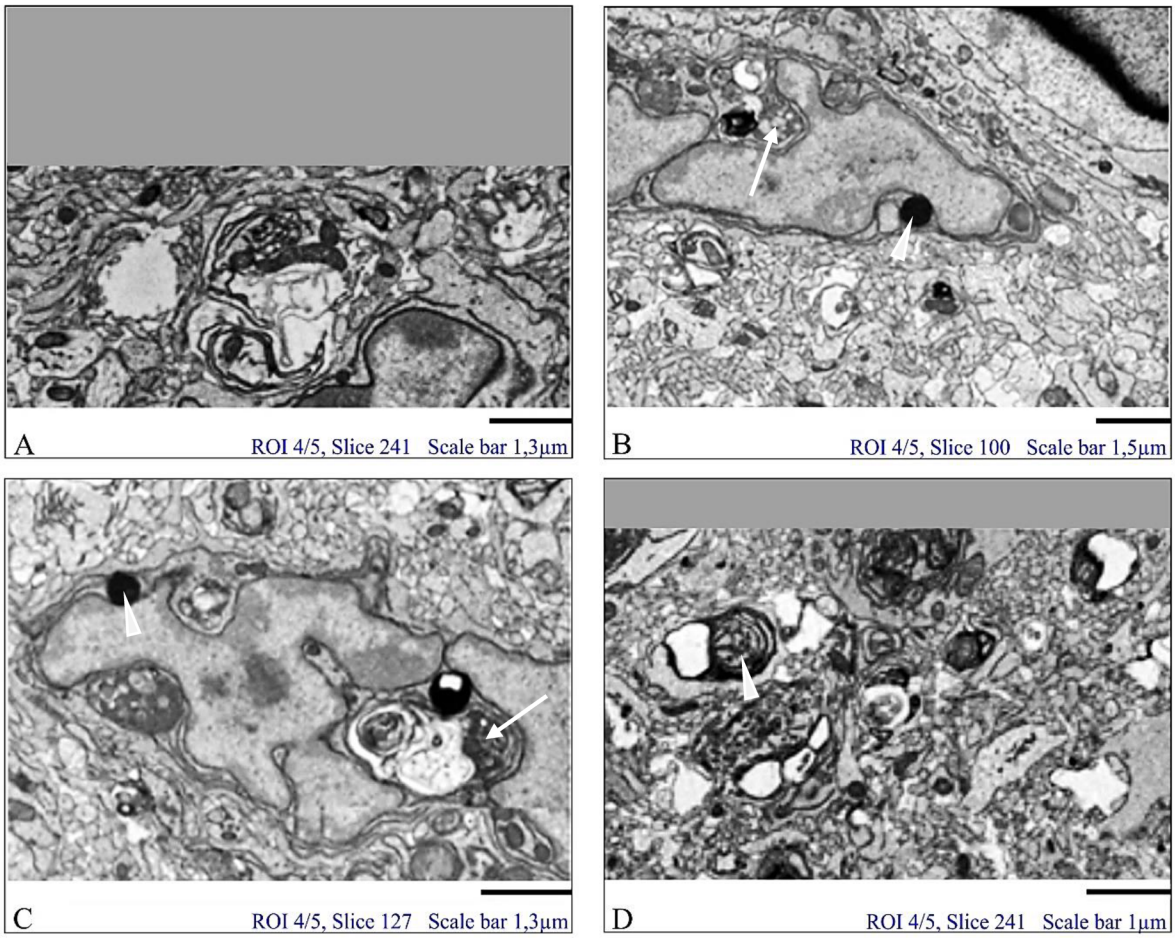

Figure 15: Various stages of necrosis (ROI4/5). Lysosomes reside near the necrotic parts (arrows). In B-C, electron-dense vacuoles should be primary lysosomes. Figure 15C shows the presumed fusion of a primary lysosome with the whorled structure. This process is shown at different depths of the cell, which probably depicts an astrocyte (15B, C). In 15D, the membranes of the whorled structures are no longer sharply delineated and merge.

Proliferation of the rough endoplasmic reticulum and cytoskeletal disintegration in response to TBEV infection were already demonstrated *in vitro* by Růžek et al. in 2009. Furthermore, Bílý et al. described proliferation of ER as well as the formation of membranous whorls *in vitro* and proposed them as autophagic vacuoles that contain TBE virions inside them (Bílý et al., 2015). However, here I show the formation of circular structures in long processes, dendrites, and astrocyte end feet, *in vivo* (Figs. 7-19).

It is known that dendrites contain free ribosomes and express satellite secretion pathways to ensure synaptic plasticity (reviewed by (Hirano et al., 2014)). Hirano et al. demonstrated that viral proteins are synthesized in the cell soma of neural cells via time-course experiments, suggesting a later transport of viral genetic material to the dendrites. The freely available ribosomes there could then be used to start replication and build membranous replication factories using the Laminal membrane (LM) as a source for the round structure (Hirano et al., 2014). IFA and TEM studies have shown that dendritic replication of flaviviruses causes abnormal neurite swelling and the development of a specific LM structure (reviewed by (Hirano et al., 2014)). In this study, it is not possible to assign exact time points since all results are just brief snapshots taken at the same timepoint of the infection. Nevertheless, here I can confirm the formation of such circular structures in dendrites and long processes *in vivo*. Also, Hirano et al. did not directly observe changes in the microtubule distribution. However, they argue that the replication factories formed disrupt microtubules in long processes and thereby obstruct trafficking pathways, which they justified by inhibiting microtubules through nocodazole treatment, resulting in decreased viral infectivity (Hirano et al., 2014). According to my observations, the round structures formed in long processes, far from the cell soma (Fig. 9D). In the body of nerve cells and in the proximal dendrites, the rough endoplasmic reticulum dominates, while in the distal parts of dendrites and dendrite spines, the smooth ER is prominent (Spacek & Harris, 1996), indicating that it is possible that in this study the observed whorls were created using the smooth ER as a membrane source. The formation of ER whorls was already shown in yeast upon inducing ER stress (Fig. 16) (Bernales et al., 2006). The microautophagy of the whorls has been proposed as a mechanism to counterbalance ER expansion induced by excessive accumulation of unfolded proteins (Schuck et al., 2014). Autophagy is the transport of constituents of the cytoplasm into

lysosomes. Cells usually use this process for many purposes, such as selective removal of damaged or no longer needed organelles (Klionsky, 2005). Given, that viral infection and its replication induce cell stress, causing autophagy to occur as a frequent by-product of viral infection (Senft & Ronai, 2015), my data suggests that the whorls observed could be of autophagic origin (Fig. 9E, 9F). Beránková et al. proposed a time-dependent role of autophagy in PMJ-2 cells during TBEV infection, proposing an antiviral early stage and a later stage that promotes replication (Beránková et al., 2022). Therefore, autophagy is sometimes successful and inhibits replication through lysosomal fusion (Figs. 12A-F), but also can lead to the formation of a spatially confined space that promotes replication (Figs. 9E-F).

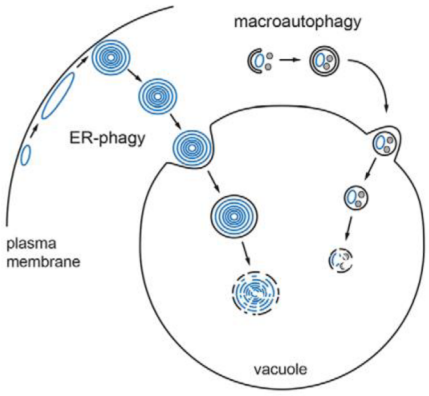

Figure 16: The autophagic response to ER stress in *Saccharomyces cervisiae*. The peripheral ER (blue) expands and forms ER whorls during ER stress. These whorls are then selectively taken up by the ER-phagy vacuoles and simultaneously macroautophagy is activated. These then form autophagosomes (crescent-shaped membrane sacs) that engulf pieces of the ER (blue) and other constituents (grey). Macroautophagy and ER-phagy might act in an independent manner and in parallel, as shown here, but could also work together (modified from Schuck et al., 2014).

It has been shown that, in human TBEV-infected neuronal glial cells, there was no upregulation of major autophagic genes, but genes involved in pyroptosis were upregulated. (Fares et al., 2021). Pyroptosis is a recently discovered regulated form of necrosis. The growing evidence indicates that the host's autophagy is disrupted to modulate the life cycles of flaviviruses, including hepatitis C, Japanese encephalitis, Dengue, Zika, and West Nile virus (Ke, 2018) Also viruses from other viral families are known to affect autophagy using different strategies (Ke, 2018, Lennemann & Coyne, 2015). However, in human astrocytes, the infectiousness of pathogenic flaviviruses (TBEVs and WNVs) is reflected in an increased rate of autophagy, while, on the contrary, the replication of flaviviruses appears to be independent of autophagy in this cell type (Tavčar Verdev et al., 2022).

4.2. Infection of endothelial cells

Throughout the entire sample volume (203 435.5 μm^3), I observed only two damaged endothelial cells (Fig. 17A, 17B), which show a lower electron density of their cytoplasm. In Figure 17 B, endothelial cells with different electron density can be compared. In the endothelium, I did not find any viruses or typical ultrastructural changes induced by TBEV infection described in in vitro studies (Růžek et al., 2009) (Bílý et al., 2015) except for several vesicles containing presumable virions, of which three examples are shown in (Figs. 18 A-C). In Fig. 18C, the only case where such a vesicle is present in the ER cisternae is shown. The low rate of damaged endothelial cells supports the hypothesis that TBEV is transcellularly transported through endothelial cells without their infection. This is in agreement with the few reports of *in vivo* infection of BBB endothelial cells by flaviviruses (Velandia-Romero et al., 2012).

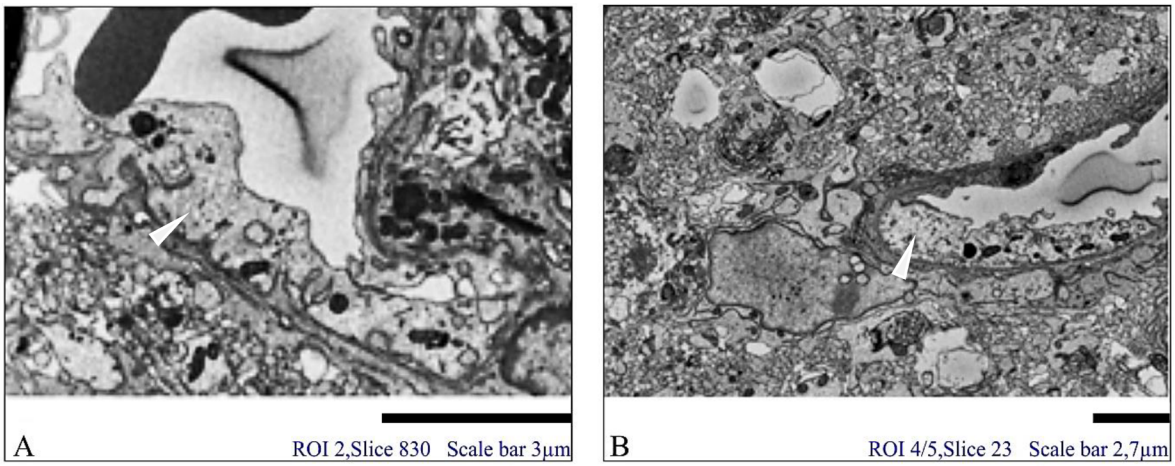

Figure 17: Overview and detailed view of endothelial cells with lower electron density of the cytoplasm (arrowheads) (ROI2 A), (ROI 4/5 B).

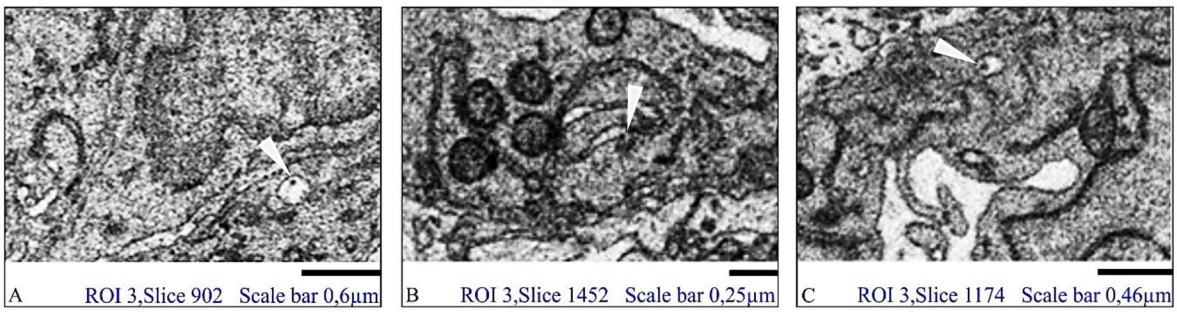

Figure 18: Possible virion particles in the endothelium (ROI3). In Figure A, a vesicle containing a black dot is in a vacuole next to the ER cisternae, whereas Figure B shows as possible virion in the proliferated ER itself. Figure C presents such a vesicle in the ER lumen (arrowheads).

4.3. Involvement of the BBB – Alterations in cells and necrotic areas surrounding the capillary

Due to the possibility to observe cells located near the capillary (their shape and internal structures) at different depths of the specimen block, I assume that most TBEV infected cells were astrocytes that contact capillaries via projections named end feet. Numerous infected astrocytes contained altered internal structures and their end feet which were in contact with the capillary (Fig. 19 A-C) . This may indicate their susceptibility to infection. In many areas around the capillaries, I found the space around the capillary to be 'empty', suggesting necrosis of astrocytes (Fig. 20A-E).

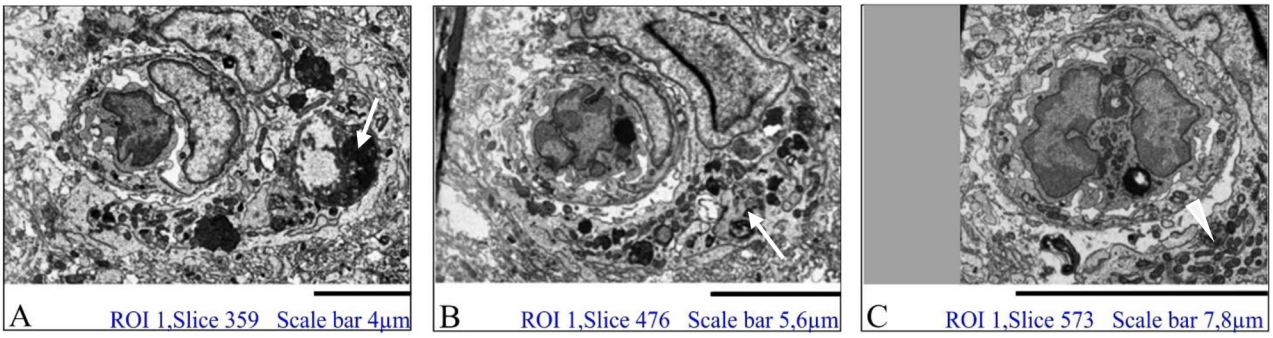

Figure 19: Capillary (ROI1) surrounded with altered cells shown at different depths of tissue. In the capillary, a macrophage is visible of which two appeared in the whole examined volume. The necrotic cell (Fig. 19, arrow) and an astrocytic end foot can be observed in the lower half of the capillary (arrowhead). Furthermore, the cell surrounding the necrotic parts has alterations such as numerous secondary lysosomes and visible chromatin disintegration (Fig. 19A) (arrow).

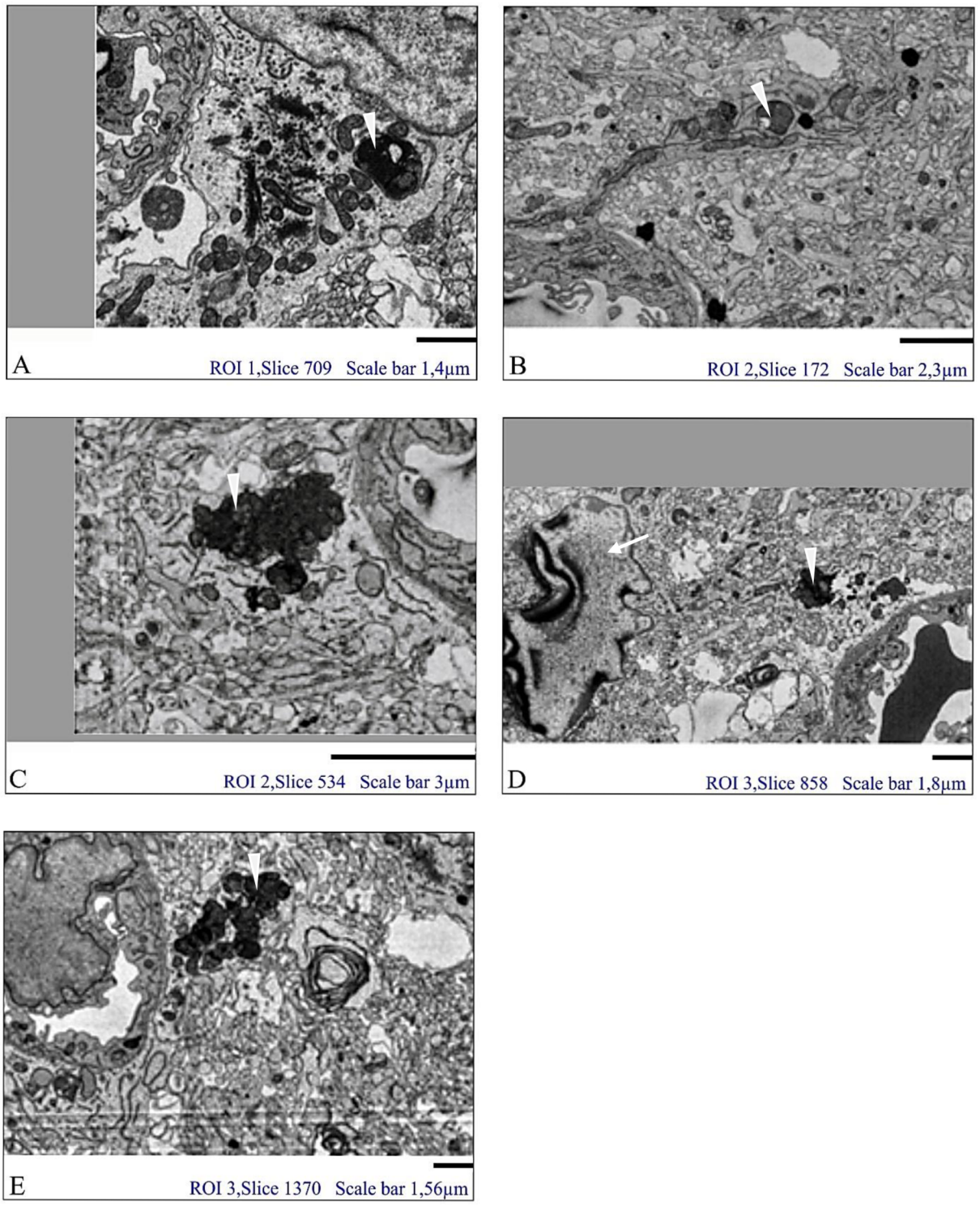

Figure 20: Infected perivascular astrocytes and their end-feet-enveloping brain capillaries (ROI1 A), (ROI2 B, C), (ROI3 D, E). In the end-feet of astrocytes (arrow) in TBEV infected brain tissue often contained large secondary lysosomes (Fig. 20 A-E) (arrowheads).

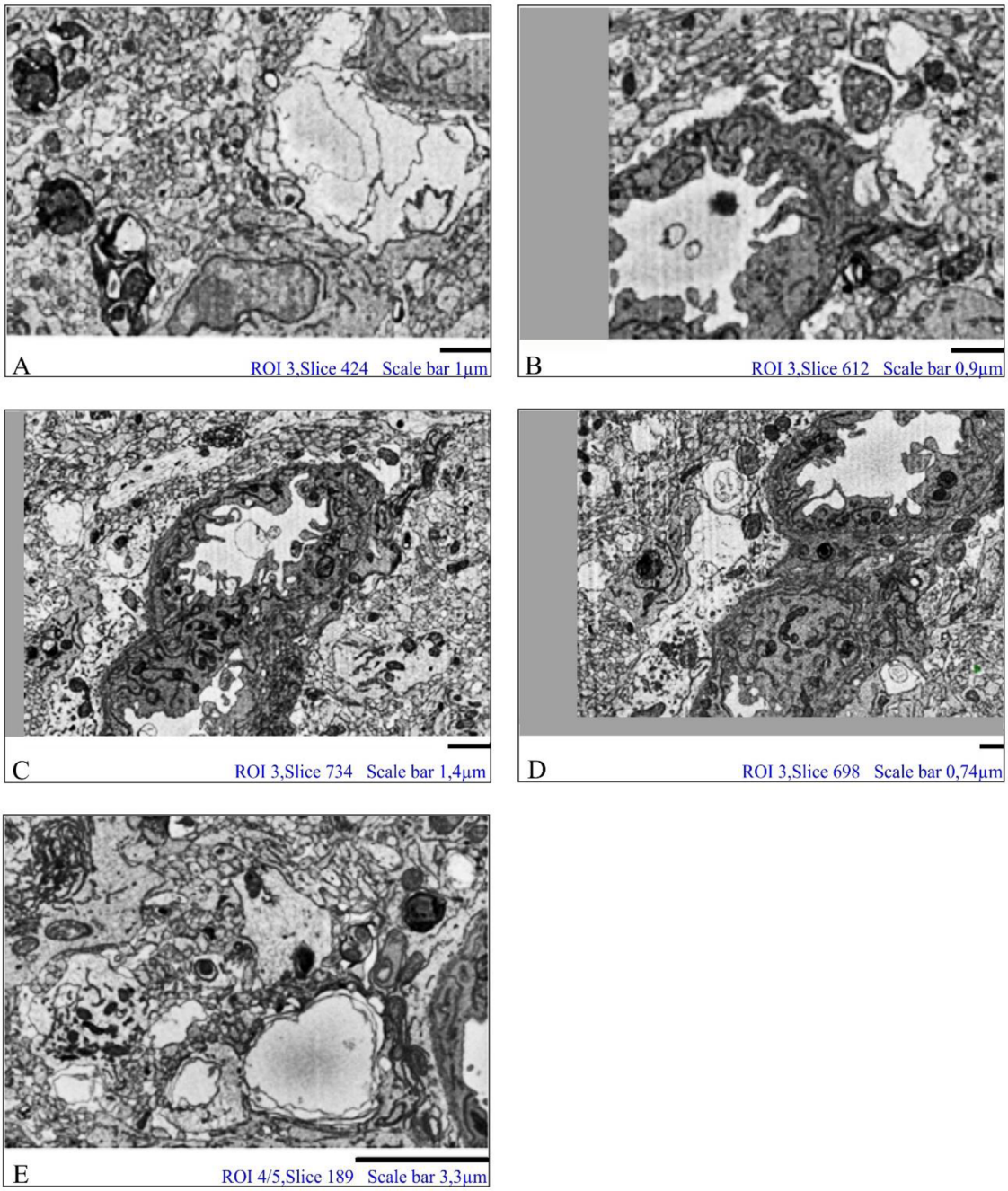

Figure 21: Necrosis near the capillary. Large empty spaces occurred next to the basal lamina (Fig. 21 A-D) or in the proximate brain tissue (Fig. 21 E).

Astrocytes have been shown to play a role as reservoir of TBEV infection in rodents (reviewed by (Potokar et al., 2019)), as shown in (Fig. 8), where replication is visible in an astrocyte. The observations presented show necrosis of astrocytes and their feet, which could be due to the fact that the infection in the observed area was severe.

Astrocytes can also maintain a protective role during infection by restricting replication ((Lindqvist et al., 2016), (Lindqvist et al., 2018)). TBEV activates astrocytes and is capable of persistently infecting them, resulting in reactive astrogliosis (Pekny & Pekna, 2016) which presents itself as a drastic functional and morphological transformation (reviewed by (Liddelow & Barres, 2017)). Reactive astrocytes can be beneficial in the sense that they remove toxic molecules, restore the BBB, and promote axonal growth and repair by the expression of components of the extracellular matrix. (reviewed by (Sofroniew, 2009)). In this process, cytokines and chemokines are also produced that activate immune cells and contribute to inflammation.

I suggest a loss of proper interaction between infected astrocytes and the BBB, as shown in Figs. 19-21, where the tight connection between astrocytes and the capillary was no longer provided, probably as a result of necrosis. Astrocytes are usually tightly connected to the endothelial cell layer and help maintain the BBB; alteration in the function of astrocytes affects the permeability of the BBB ((Abbott et al., 2006); (Yao & Tsirka, 2014)). Furthermore, necrosis in astrocyte processes, as well as lysosomal accumulation, might indicate that cells lost their function to some extent or even fully. This could be due to the fact that the infection in the observed area was severe. Astrocytes also play a role in immunopathological processing in the CNS and can contribute to the degradation of the BBB by producing matrix metalloproteinase 9 (reviewed by (Elsterová, 2020). As a result, the observed damage could have been caused by the host immune system in response to released cytokines and chemokines, which could also have affected previously healthy tissues.

5. Conclusion

By analysing the effects of TBEV infection on brain tissue, as well as the blood-brain barrier in detail, this study has shown that although TBEV was administered intracranially, it can be observed how individual cell types are susceptible to infection and how they respond to infection. The low rate of TBEV infection in endothelial cells observed throughout the sample volume (203 435.5 μm^3) corresponds to the few reports showing infection of BBB endothelial cells by flaviviruses in vivo (Velandia-Romero et al., 2012). Therefore, my findings support the hypothesis of virus transcytosis through endothelial cells without infection as the primary target of the virus.

My findings also show the involvement of autophagy in the replication process, causing extensive rebuilding of the endoplasmic reticulum which resulted in the formation of membranous whorls. I also show ER to lysosome-associated degradation in the whole sample volume *in vivo*. To the best of my knowledge, the latter process has not yet been described in relation to TBEV infection.

This study demonstrates the effects of TBEV following intracranial injection in a mouse model, and provides insights into the specific cellular responses of the brain and immune system to the virus at the ultrastructural level. However, to better understand the implications of these results, future studies could address time points during infection, such as virus entry in very early stages, to further examine endothelial involvement during the natural way of brain infection by TBEV. In conclusion, SBF-SEM is a powerful EM technique for imaging large volumes of tissue, while still achieving sufficient resolution to observe individual viruses.

6. References

Abbott, N. J., Patabendige, A. A. K., Dolman, D. E. M., Yusof, S. R., & Begley, D. J. (2010). Structure and function of the blood-brain barrier. In *Neurobiology of Disease* (Vol. 37, Issue 1, pp. 13–25). https://doi.org/10.1016/j.nbd.2009.07.030

Amicizia, D., Domnich, A., Panatto, D., Lai, P. L., Cristina, M. L., Avio, U., & Gasparini, R. (2013). Epidemiology of tick-borne encephalitis (TBE) in Europe and its prevention by available vaccines. In *Human Vaccines and Immunotherapeutics* (Vol. 9, Issue 5, pp. 1163–1171). https://doi.org/10.4161/hv.23802

Belevich, I., Joensuu, M., Kumar, D., Vihinen, H., & Jokitalo, E. (2016). Microscopy Image Browser: A Platform for Segmentation and Analysis of Multidimensional Datasets. *PLOS Biology*, *14*(1), e1002340. https://doi.org/10.1371/journal.pbio.1002340

Beránková, Z., Kopecký, J., Kobayashi, S., & Lieskovská, J. (2022). Dual control of tick-borne encephalitis virus replication by autophagy in mouse macrophages. *Virus Research*, *315*. https://doi.org/10.1016/j.virusres.2022.198778

Bernales, S., McDonald, K. L., & Walter, P. (2006). Autophagy Counterbalances Endoplasmic Reticulum Expansion during the Unfolded Protein Response. *PLoS Biology*, *4*(12), e423. https://doi.org/10.1371/journal.pbio.0040423

Bhide, K., Mochnáčová, E., Tkáčová, Z., Petroušková, P., Kulkarni, A., & Bhide, M. (2022). Signaling events evoked by domain III of envelop glycoprotein of tick-borne encephalitis virus and West Nile virus in human brain microvascular endothelial cells. *Scientific Reports*, *12*(1). https://doi.org/10.1038/s41598-022-13043-1

Bílý, T., Palus, M., Eyer, L., Elsterová, J., Vancová, M., & Růžek, D. (2015). Electron Tomography Analysis of Tick-Borne Encephalitis Virus Infection in Human Neurons. *Scientific Reports*, *5*. https://doi.org/10.1038/srep10745

Bogovic, P. (2015). Tick-borne encephalitis: A review of epidemiology, clinical characteristics, and management. *World Journal of Clinical Cases*, *3*(5), 430. https://doi.org/10.12998/wjcc.v3.i5.430

Bogovič, P., Kastrin, A., Lotrič-Furlan, S., Ogrinc, K., Avšič Županc, T., Korva, M., Knap, N., Resman Rus, K., Strle, K., & Strle, F. (2022). Comparison of laboratory and immune characteristics of the initial and second phase of tick-borne encephalitis. *Emerging Microbes and Infections*, *11*(1), 1647–1656. https://doi.org/10.1080/22221751.2022.2086070

Bogovič, P., Kastrin, A., Lotrič-Furlan, S., Ogrinc, K., Županc, T. A., Korva, M., Knap, N., & Strle, F. (2022). Clinical and Laboratory Characteristics and Outcome of Illness Caused by Tick-Borne Encephalitis Virus without Central Nervous System Involvement. *Emerging Infectious Diseases*, *28*(2), 291–301. https://doi.org/10.3201/eid2802.211661

Bradl, M., & Lassmann, H. (2010). Oligodendrocytes: Biology and pathology. In *Acta Neuropathologica* (Vol. 119, Issue 1, pp. 37–53). https://doi.org/10.1007/s00401-009-0601-5

Chmielewska, A. M., Gómez-Herranz, M., Gach, P., Nekulova, M., Bagnucka, M. A., Lipi Nska, A. D., Rychłowski, M., Hoffmann, W., Król, E., Vojtesek, B., Sloan, R. D., Bie Nkowska-Szewczyk, K., Hupp, T., & Ball, K. (2022). *The Role of IFITM Proteins in Tick-Borne Encephalitis Virus Infection*. https://journals.asm.org/journal/jvi

Coomber' And, B. L., & Stewart, P. A. (1985). Morphometric Analysis of CNS Microvascular Endothelium. In *MICROVASCULAR RESEARCH* (Vol. 30).

Courson, J. A., Landry, P. T., Do, T., Spehlmann, E., Lafontant, P. J., Patel, N., Rumbaut, R. E., & Burns, A. R. (2021). Serial Block-Face Scanning Electron Microscopy (SBF-SEM) of Biological Tissue Samples. *Journal of Visualized Experiments*, *169*. https://doi.org/10.3791/62045

Daneman, R. (2012). The blood-brain barrier in health and disease. *Annals of Neurology*, *72*(5), 648–672. https://doi.org/10.1002/ana.23648

Daneman, R., & Prat, A. (2015). The blood–brain barrier. *Cold Spring Harbor Perspectives in Biology*, *7*(1). https://doi.org/10.1101/cshperspect.a020412

Deerinck, T., Bushong, E., Lev-Ram, V., Shu, X., Tsien, R., & Ellisman, M. (2010). Enhancing Serial Block-Face Scanning Electron Microscopy to Enable High Resolution 3-D Nanohistology of Cells and Tissues. *Microscopy and Microanalysis*, *16*(S2), 1138–1139. https://doi.org/10.1017/S1431927610055170

Dobler, G. (2010). Zoonotic tick-borne flaviviruses. In *Veterinary Microbiology* (Vol. 140, Issues 3–4, pp. 221–228). https://doi.org/10.1016/j.vetmic.2009.08.024

Dobler, G., Erber, W., & Bröker, M. (2021). *The TBE book* (Vol. 4th). Global Health Press.

Dobler G, & Tkachev S. (2021). *General epidemiology of TBE* (Dobler G, Erber W, Bröker M, & Schmitt HJ, Eds.; 4th edition). Global Health Press.

Fares, M., Gorna, K., Berry, N., Cochet-bernoin, M., Piumi, F., Blanchet, O., Haddad, N., Richardson, J., & Coulpier, M. (2021). Transcriptomic studies suggest a coincident role for apoptosis and pyroptosis but not for autophagic neuronal death in tbev-infected human neuronal/glial cells. *Viruses*, *13*(11). https://doi.org/10.3390/v13112255

Füzik, T., Formanová, P., Růžek, D., Yoshii, K., Niedrig, M., & Plevka, P. (2018). Structure of tick-borne encephalitis virus and its neutralization by a monoclonal antibody. *Nature Communications*, *9*(1). https://doi.org/10.1038/s41467-018-02882-0

Gingrich, M. B., & Traynelis, S. F. (2000). Serine proteases and brain damage – is there a link? *Trends in Neurosciences*, *23*(9), 399–407. https://doi.org/10.1016/S0166-2236(00)01617-9

Hawkins, B. T., & Davis, T. P. (2005). The blood-brain barrier/neurovascular unit in health and disease. In *Pharmacological Reviews* (Vol. 57, Issue 2, pp. 173–185). https://doi.org/10.1124/pr.57.2.4

Hirano, M., Yoshii, K., Sakai, M., Hasebe, R., Ichii, O., & Kariwa, H. (2014). Tick-borne flaviviruses alter membrane structure and replicate in dendrites of primary mouse neuronal cultures. *Journal of General Virology*, *95*(PART 4), 849–861. https://doi.org/10.1099/vir.0.061432-0

Kadry, H., Noorani, B., & Cucullo, L. (2020). A blood–brain barrier overview on structure, function, impairment, and biomarkers of integrity. In *Fluids and Barriers of the CNS* (Vol. 17, Issue 1). BioMed Central Ltd. https://doi.org/10.1186/s12987-020-00230-3

Ke, P.-Y. (2018). The Multifaceted Roles of Autophagy in Flavivirus-Host Interactions. *International Journal of Molecular Sciences*, *19*(12), 3940. https://doi.org/10.3390/ijms19123940

Klionsky, D. J. (2005). The molecular machinery of autophagy: unanswered questions. *Journal of Cell Science*, *118*(1), 7–18. https://doi.org/10.1242/jcs.01620

Kohlmaier, B., Schweintzger, N. A., Sagmeister, M. G., Švendová, V., Kohlfürst, D. S., Sonnleitner, A., Leitner, M., Berghold, A., Schmiedberger, E., Fazekas, F., Pichler, A., Rejc-Marko, J., Růžek, D., Dufková, L., Čejková, D., Husa, P., Pýchová, M., Krbková, L., Chmelík, V., … Zenz, W. (2021). Clinical characteristics of patients with tick-borne encephalitis (Tbe): A european multicentre

study from 2010 to 2017. *Microorganisms*, *9*(7). https://doi.org/10.3390/microorganisms9071420

Koyuncu, O. O., Hogue, I. B., & Enquist, L. W. (2013). Virus Infections in the Nervous System. *Cell Host & Microbe*, *13*(4), 379–393. https://doi.org/10.1016/j.chom.2013.03.010

Kutschera, L. S., & Wolfinger, M. T. (n.d.). *Evolutionary traits of Tick-borne encephalitis virus: Pervasive non-coding RNA structure conservation and molecular epidemiology*. https://doi.org/10.1101/2021.12.16.473019

Labuda, M., Austyn, J. M., Zuffova, E., Kozuch, O., Fuchsberger, N., Lysy, J., & Nuttall, P. A. (1996). Importance of Localized Skin Infection in Tick-Borne Encephalitis Virus Transmission. In *VIROLOGY* (Vol. 219).

Lennemann, N. J., & Coyne, C. B. (2015). Catch Me If You Can: The Link between Autophagy and Viruses. *PLOS Pathogens*, *11*(3), e1004685. https://doi.org/10.1371/journal.ppat.1004685

Liddelow, S. A., & Barres, B. A. (2017). Reactive Astrocytes: Production, Function, and Therapeutic Potential. *Immunity*, *46*(6), 957–967. https://doi.org/10.1016/j.immuni.2017.06.006

Lieskovská, J., Páleníková, J., Langhansová, H., Chmelař, J., & Kopecký, J. (2018). Saliva of Ixodes ricinus enhances TBE virus replication in dendritic cells by modulation of pro-survival Akt pathway. *Virology*, *514*, 98–105. https://doi.org/10.1016/j.virol.2017.11.008

Lindqvist, R., Kurhade, C., Gilthorpe, J. D., & Överby, A. K. (2018). Cell-type- and region-specific restriction of neurotropic flavivirus infection by viperin. *Journal of Neuroinflammation*, *15*(1), 80. https://doi.org/10.1186/s12974-018-1119-3

Lindqvist, R., Mundt, F., Gilthorpe, J. D., Wölfel, S., Gekara, N. O., Kröger, A., & Överby, A. K. (2016). Fast type I interferon response protects astrocytes from flavivirus infection and virus-induced cytopathic effects. *Journal of Neuroinflammation*, *13*(1), 277. https://doi.org/10.1186/s12974-016-0748-7

Ludlow, M., Kortekaas, J., Herden, C., Hoffmann, B., Tappe, D., Trebst, C., Griffin, D. E., Brindle, H. E., Solomon, T., Brown, A. S., van Riel, D., Wolthers, K. C., Pajkrt, D., Wohlsein, P., Martina, B. E. E., Baumgärtner, W., Verjans, G. M., & Osterhaus, A. D. M. E. (2016). Neurotropic virus infections as the cause of immediate and delayed neuropathology. In *Acta Neuropathologica* (Vol. 131, Issue 2, pp. 159–184). Springer Verlag. https://doi.org/10.1007/s00401-015-1511-3

Mandl, C. W. (2005). Steps of the tick-borne encephalitis virus replication cycle that affect neuropathogenesis. In *Virus Research* (Vol. 111, Issue 2 SPEC. ISS., pp. 161–174). Elsevier. https://doi.org/10.1016/j.virusres.2005.04.007

Martello, E., Gillingham, E. L., Phalkey, R., Vardavas, C., Nikitara, K., Bakonyi, T., Gossner, C. M., & Leonardi-Bee, J. (2022). Systematic review on the non-vectorial transmission of Tick-borne encephalitis virus (TBEv). In *Ticks and Tick-borne Diseases* (Vol. 13, Issue 6). Elsevier GmbH. https://doi.org/10.1016/j.ttbdis.2022.102028

McMinn, P. C. (1997). The molecular basis of virulence of the encephalitogenic flaviviruses. *Journal of General Virology*, *78*(11), 2711–2722. https://doi.org/10.1099/0022-1317-78-11-2711

Mennicken, F., Maki, R., de Souza, E. B., & Quirion, R. (1999). Chemokines and chemokine receptors in the CNS: a possible role in neuroinflammation and patterning. *Trends in Pharmacological Sciences*, *20*(2), 73–78. https://doi.org/10.1016/S0165-6147(99)01308-5

Miorin, L., Romero-Brey, I., Maiuri, P., Hoppe, S., Krijnse-Locker, J., Bartenschlager, R., & Marcello, A. (2013). Three-Dimensional Architecture of Tick-Borne Encephalitis Virus Replication Sites and

Trafficking of the Replicated RNA. *Journal of Virology*, *87*(11), 6469–6481. https://doi.org/10.1128/jvi.03456-12

Nadal, A., Fuentes, E., Pastor, J., & McNaughton, P. A. (1995). Plasma albumin is a potent trigger of calcium signals and DNA synthesis in astrocytes. *Proceedings of the National Academy of Sciences*, *92*(5), 1426–1430. https://doi.org/10.1073/pnas.92.5.1426

Nguyen-Dinh, V., & Herker, E. (2021). Ultrastructural features of membranous replication organelles induced by positive-stranded RNA viruses. In *Cells* (Vol. 10, Issue 9). MDPI. https://doi.org/10.3390/cells10092407

Överby, A. K., Popov, V. L., Niedrig, M., & Weber, F. (2010). Tick-Borne Encephalitis Virus Delays Interferon Induction and Hides Its Double-Stranded RNA in Intracellular Membrane Vesicles. *Journal of Virology*, *84*(17), 8470–8483. https://doi.org/10.1128/jvi.00176-10

Palus, M., Vancova, M., Sirmarova, J., Elsterova, J., Perner, J., & Ruzek, D. (2017). Tick-borne encephalitis virus infects human brain microvascular endothelial cells without compromising blood-brain barrier integrity. *Virology*, *507*, 110–122. https://doi.org/10.1016/j.virol.2017.04.012

Peddie, C. J., & Collinson, L. M. (2014). Exploring the third dimension: Volume electron microscopy comes of age. *Micron*, *61*, 9–19. https://doi.org/10.1016/j.micron.2014.01.009

Potokar, M., Jorgačevski, J., & Zorec, R. (2019). Astrocytes in flavivirus infections. In *International Journal of Molecular Sciences* (Vol. 20, Issue 3). MDPI AG. https://doi.org/10.3390/ijms20030691

Pulkkinen, L. I. A., Butcher, S. J., & Anastasina, M. (2018). Tick-borne encephalitis virus: A structural view. In *Viruses* (Vol. 10, Issue 7). MDPI AG. https://doi.org/10.3390/v10070350

RNDr Jana Elsterová Supervisor, thesis, & RNDr Daniel Růžek, doc. (n.d.). *Pathogenesis and clinical aspects of tick-borne encephalitis virus infection*.

Romero-Brey, I., & Bartenschlager, R. (2014). Membranous replication factories induced by plus-strand RNA viruses. In *Viruses* (Vol. 6, Issue 7, pp. 2826–2857). MDPI AG. https://doi.org/10.3390/v6072826

Růžek, D., Salát, J., Singh, S. K., & Kopecký, J. (2011). Breakdown of the blood-brain barrier during tick-borne encephalitis in mice is not dependent on CD8+ T-cells. *PLoS ONE*, *6*(5). https://doi.org/10.1371/journal.pone.0020472

Růžek, D., Vancová, M., Tesařová, M., Ahantarig, A., Kopecký, J., & Grubhoffer, L. (2009). Morphological changes in human neural cells following tick-borne encephalitis virus infection. *Journal of General Virology*, *90*(7), 1649–1658. https://doi.org/10.1099/vir.0.010058-0

Schuck, S., Gallagher, C. M., & Walter, P. (2014). ER-phagy mediates selective degradation of endoplasmic reticulum independently of the core autophagy machinery. *Journal of Cell Science*. https://doi.org/10.1242/jcs.154716

Senft, D., & Ronai, Z. A. (2015). UPR, autophagy, and mitochondria crosstalk underlies the ER stress response. *Trends in Biochemical Sciences*, *40*(3), 141–148. https://doi.org/10.1016/j.tibs.2015.01.002

Sofroniew, M. V. (2009). Molecular dissection of reactive astrogliosis and glial scar formation. *Trends in Neurosciences*, *32*(12), 638–647. https://doi.org/10.1016/j.tins.2009.08.002

Spacek, J., & Harris, K. M. (1996). *Three-Dimensional Organization of Smooth Endoplasmic Reticulum in Hippocampal CA1 Dendrites and Dendritic Spines of the Immature and Mature Rat*.

Stamatovic, S. M., Shakui, P., Keep, R. F., Moore, B. B., Kunkel, S. L., van Rooijen, N., & Andjelkovic, A. v. (2005). Monocyte Chemoattractant Protein-1 Regulation of Blood–Brain Barrier Permeability. *Journal of Cerebral Blood Flow & Metabolism*, *25*(5), 593–606. https://doi.org/10.1038/sj.jcbfm.9600055

Sudhindra, P. (2018). Tick-Borne Infections of the Central Nervous System. In *The Microbiology of Central Nervous System Infections* (pp. 173–195). Elsevier. https://doi.org/10.1016/b978-0-12-813806-9.00010-x

Tapia, J. C., Kasthuri, N., Hayworth, K. J., Schalek, R., Lichtman, J. W., Smith, S. J., & Buchanan, J. (2012). High-contrast en bloc staining of neuronal tissue for field emission scanning electron microscopy. *Nature Protocols*, *7*(2), 193–206. https://doi.org/10.1038/nprot.2011.439

Tavčar Verdev, P., Potokar, M., Korva, M., Resman Rus, K., Kolenc, M., Avšič Županc, T., Zorec, R., & Jorgačevski, J. (2022). In human astrocytes neurotropic flaviviruses increase autophagy, yet their replication is autophagy-independent. *Cellular and Molecular Life Sciences*, *79*(11), 566. https://doi.org/10.1007/s00018-022-04578-7

Teijaro, J. R., Walsh, K. B., Cahalan, S., Fremgen, D. M., Roberts, E., Scott, F., Martinborough, E., Peach, R., Oldstone, M. B. A., & Rosen, H. (2011). Endothelial Cells Are Central Orchestrators of Cytokine Amplification during Influenza Virus Infection. *Cell*, *146*(6), 980–991. https://doi.org/10.1016/j.cell.2011.08.015

Velandia-Romero, M. L., Acosta-Losada, O., & Castellanos, J. E. (2012). In vivo infection by a neuroinvasive neurovirulent dengue virus. *Journal of NeuroVirology*, *18*(5), 374–387. https://doi.org/10.1007/s13365-012-0117-y

Wikel, S. K., Ramachandra, R. N., & Bergman, D. K. (1994). TICK-INDUCED MODULATION OF THE HOST IMMUNE RESPONSE. In *JournalJiw Parasilology* (Vol. 24, Issue I).

Wolburg, H., & Lippoldt, A. (n.d.). *Tight junctions of the blood-brain barrier: Development, composition and regulation*. https://www.researchgate.net/publication/292768551

Woodruff, A. (n.d.). *What is a neuron?* Https://Qbi.Uq.Edu.Au/Brain/Brain-Anatomy/What-Neuron.

Yao, Y., & Tsirka, S. E. (2014). Monocyte chemoattractant protein-1 and the blood–brain barrier. *Cellular and Molecular Life Sciences*, *71*(4), 683–697. https://doi.org/10.1007/s00018-013-1459-1

Zlokovic, B. v. (2008). The Blood-Brain Barrier in Health and Chronic Neurodegenerative Disorders. *Neuron*, *57*(2), 178–201. https://doi.org/10.1016/j.neuron.2008.01.003